Journal of Medicinal Chemistry

Article

Discovery of 2-{3-[2-(1-isopropyl-3-methyl-1H-1,2-4-triazol-5-yl)-5,6-dihydrobenzo[f]imidazo[1,2-d][1,4]oxazepin-9-yl]-1H-pyrazol-1-yl}-2-methylpropanamide (GDC-0032): A #-sparing phosphoinositide 3-kinase (PI3K) inhibitor with high unbound exposure and robust in vivo anti-tumor activity

Chudi Ndubaku, Timothy P Heffron, Steven Thomas Staben, Matthew Baumgardner, Nicole Blaquiere, Erin Bradley, Richard Bull, Steven Do, Jennafer Dotson, Danette Dudley, Kyle Edgar, Lori Friedman, Richard Goldsmith, Robert Andrew Heald, Aleks Kolesnikov, Leslie Lee, Cristina Lewis, Michelle Nannini, Jim Nonomiya, Jodie Pang, Steve Price, Wei Wei Prior, Laurent Salphati, Steve Sideris, Jeffrey Wallin, Lan Wang, Binqing Wei, Deepak Sampath, and Alan G Olivero

J. Med. Chem., **Just Accepted Manuscript** • DOI: 10.1021/jm4003632 • Publication Date (Web): 10 May 2013

Just Accepted

Journal of Medicinal Chemistry is published by the American Chemical Society. 1155 Sixteenth Street N.W., Washington, DC 20036

Discovery of 2-{3-[2-(1-isopropyl-3-methyl-1H-1,2-4-triazol-5-yl)-5,6-dihydrobenzo[f]imidazo[1,2-d][1,4]oxazepin-9-yl]-1H-pyrazol-1-yl}-2-methylpropanamide (GDC-0032): A β-sparing phosphoinositide 3-kinase (PI3K) inhibitor with high unbound exposure and robust in vivo anti-tumor activity

Chudi O. Ndubaku,[‡] Timothy P. Heffron,*[‡] Steven T. Staben,[‡] Matthew Baumgardner,[†] Nicole Blaquiere,[‡] Erin Bradley,[‡] Richard Bull,[∫] Steven Do,[‡] Jennafer Dotson,[‡] Danette Dudley,[‡] Kyle A. Edgar,[¶] Lori S. Friedman,[¶] Richard Goldsmith,[‡] Robert A. Heald,[∫] Aleksandr Kolesnikov,[‡] Leslie Lee,[¶] Cristina Lewis,[§] Michelle Nannini,[¶] Jim Nonomiya,[§] Jodie Pang,[†] Steve Price,[∫] Wei Wei Prior,[¶,°] Laurent Salphati,[†] Steve Sideris,[§] Jeffery J. Wallin,[¶] Lan Wang,[‡] BinQing Wei,[‡] Deepak Sampath,[¶] Alan G. Olivero[‡]

Departments of [‡]Discovery Chemistry, [†]Drug Metabolism and Pharmacokinetics, [¶]Translational Oncology, and [§]Biochemical Pharmacology, Genentech, Inc., 1 DNA Way, South San Francisco, CA 94080, USA; [∫]Argenta Discovery, 8-9 Spire Green Centre, Flex Meadow, Harlow, Essex, CM19 5TR, UK

RECEIVED DATE (to be automatically inserted after your manuscript is accepted if required according to the journal that you are submitting your paper to)

Abstract

Dysfunctional signaling through the PI3K/AKT/mTOR pathway leads to uncontrolled tumor proliferation. In the course of the discovery of novel benzoxepin PI3K inhibitors, we observed a strong dependency of in vivo anti-tumor activity on the free drug exposure. By lowering the intrinsic clearance, we derived a set of imidazobenzoxazepin compounds that showed improved unbound drug exposure and effectively suppressed growth of tumors in a mouse xenograft model at low drug dose levels. One of these compounds, GDC-0032 (**11l**), was progressed to clinical trials and is currently under Phase I evaluation as a potential treatment for human malignancies.

Introduction

The phosphoinositide 3-kinase (PI3K) enzymes are lipid kinases responsible for the conversion of membrane-bound 4,5-phosphatidylinositolbisphosphate (PIP2) into 3,4,5-phosphatidylinositoltrisphosphate (PIP3).[1,2] This signaling event occurs in response to various extracellular triggers including activation of receptor tyrosine kinases (RTKs) and G-protein coupled receptors (GPCRs). Phosphorylation to PIP3 in turn promotes downstream activation of Akt and mTOR, which influence several functions important to cellular integrity including proliferation, evasion of apoptosis, metabolism and angiogenesis. Not surprisingly, perturbations of this crucial pathway are highly associated with cancer. While there are four class I PI3K isoforms (α, β, δ and γ) implicated in the signaling cascade, the aberration most common to cancer is the amplification or activating mutation of PI3Kα.[3-5] Moreover, inactivation or genetic deletion of the negative regulator of this pathway, phosphatase and tensin homolog (PTEN), is also common.[6] As a result, small molecule inhibitors that target the PI3Ks have been intensely pursued as potential treatments for various types of cancers and some of these have recently advanced into the clinic.[7,8]

Table 1. Comparison of clinical compound GDC-0941 **(1)** and thiazolobenzoxepin **2**

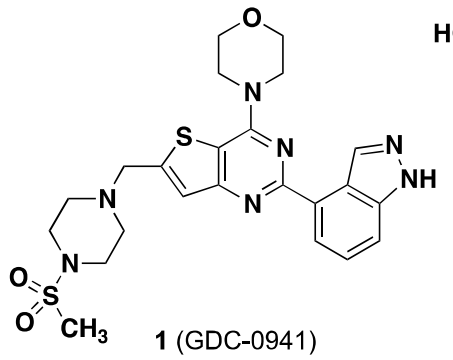

1 (GDC-0941)

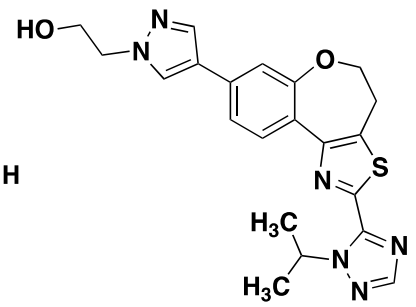

2

Compound	PI3Kα IC_{50} (nM)[a]	p-Akt (S473) IC_{50} (μM)[b]	MCF7-neo/HER2 IC_{50} (μM)[c]	cLogD[d]	Kinetic Solubility (μM)[e]	Mouse PK @ 100 mg/kg[f] AUC_{tot} (μM•h, p.o.)	Mouse PK @ 100 mg/kg[f] AUC_u (μM•h, p.o.)
1	3.0	0.007	0.290	2.1	37.0	80.3	3.5
2	< 0.5	0.016	0.195	3.8 (3.9)[g]	4.7	275	0.55

[a]IC_{50} data are an average of at least 3 independent experiments. Each value has a standard deviation of less than one geometric mean. [b]Determined with ELISA assay. [c]Cell proliferation inhibition over 72–96 h. [d]Calculated using MoKa® software. [e]Measurements carried out in PBS pH 7.2 buffer (23 ºC) with serial dilution and LC-CLND quantification. [f]Adult female nude mice were administered with compound suspended in MCT via oral gavage. [g]Measured logD value.

We recently introduced a novel class of PI3K inhibitors containing a central benzoxepin scaffold (e.g. compound **2**, Table 1).[9-12] This class of inhibitors was originally discovered by structure-guided optimization of hits from high throughput screening. Optimized compounds displayed good levels of potency towards the PI3Ks as well as high selectivity over off-targets. Strong structural rationale also exists to suggest why variations of the substituents on the benzoxepin scaffold lead to isoform selectivity for PI3Kα over PI3Kβ, an important aspect of mitigating potentially adverse effects on glucose metabolism.[10] Very recently, we showed that modifications to the heterocyclic central subunit as well as the peripheral substituents yielded drug-like compounds such as **2** (Table 1), which had sufficient exposure in vivo to achieve tumor growth inhibition (TGI) in a mouse xenograft study.[12] Despite potent in vitro activity, better

even than the clinical compound **1** (GDC-0941, Table 1),[13] **2** only achieved modest tumor growth inhibition in an MCF7-neo/HER2 xenograft breast cancer model even when dosed at its maximum absorbable dose due to solubility limitations (100 mg/kg, Figure 1A). In the graph showing the %TGI by drug dose, GDC-0941 achieves greater tumor growth inhibition at lower doses than **2** (Figure 1B). This outcome was evident despite **2** achieving significantly higher total area under the concentration–time curve (AUC_{tot}) than **1** in vivo and being slightly more potent in the proliferation assay with the same cell line evaluated in the xenograft study (Table 1). According to the free drug hypothesis, in the absence of active transport in vivo, only the steady-state unbound drug concentration available to engage the target of interest will have the ability to impart a pharmacological effect.[14] Our group had prior experience with this phenomenon during the discovery of PI3K/mTOR inhibitor GDC-0980.[15] We therefore reasoned that the minimal anti-tumor activity observed for **2** was largely due to its low solubility and limited in vivo unbound exposure achieved. The objective was then to identify molecules with improved solubility and overall lower unbound clearance (CL_u).

A.

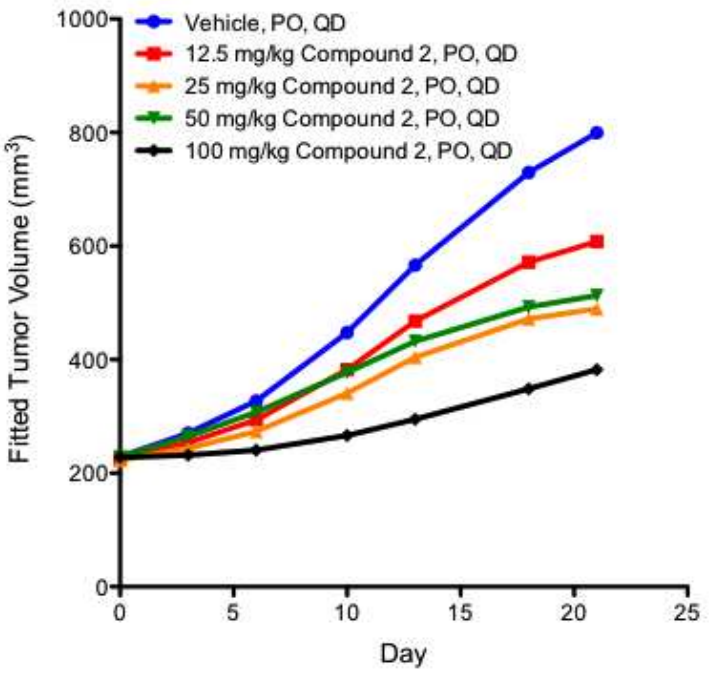

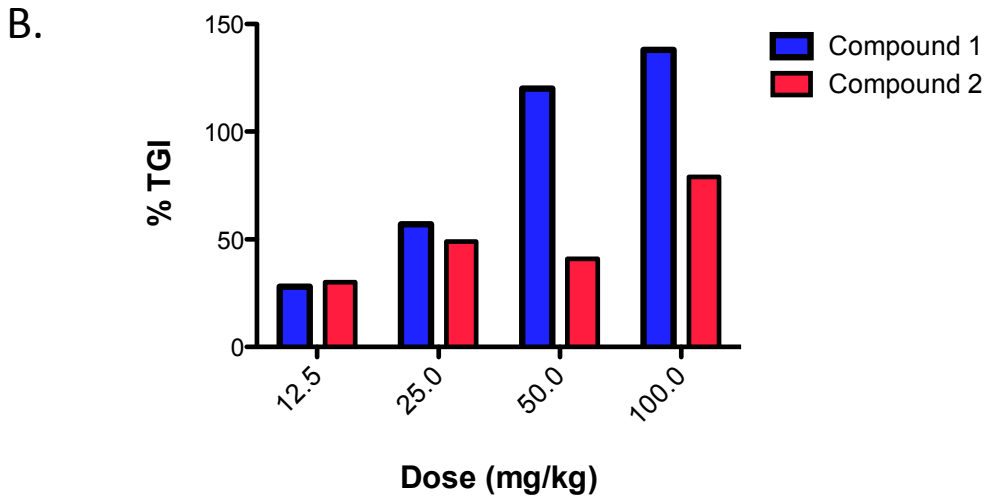

Figure 1. A) Dose-curves of tumor volume response of compound **2** against MCF7-neo/HER2 xenografts in mice relative to vehicle over the course of 21 days (0.5% methycellulose/0.2% Tween-80) B) Comparison of % tumor growth inhibition of compound **1** and **2** in MCF7-neo/HER2 xenografts at the four doses evaluated.

In order to achieve this end, we envisioned using physicochemical parameters to guide these optimizations. In particular, one property that we quickly deemed was most important was the calculated distribution coefficient (cLogD), a measure of molecular lipophilicity. While other factors such as acidity and molecular size and shape can influence properties such as in vitro protein binding and solubility, reducing cLogD has been shown to correlate with lower unbound clearance.[16] Therefore, reducing cLogD became a key strategy that we employed to increase unbound exposure in vivo. Specifically, the thiazole central subunit was targeted for modification in order to reduce overall lipophilicity.

In a previous communication,[12] we described a set of novel benzoxepin scaffolds with potent activity against PI3Kα, wherein the thiazolobenzoxepin sub-series was selected for further optimization (Figure 2). All of the scaffolds described were designed to adopt similar binding topologies in their low energy conformation and make the same requisite polar and Van der Waals interactions in the ligand-binding site. It

is important to note that for the five scaffolds (**A**–**E**) examined, the imidazobenzoxepin (**E**) was determined to have the lowest inherent cLogD value in analogous cases (e.g., • = Me, Figure 2), albeit very similar to pyrazolobenzoxazepin (**C**).[17]

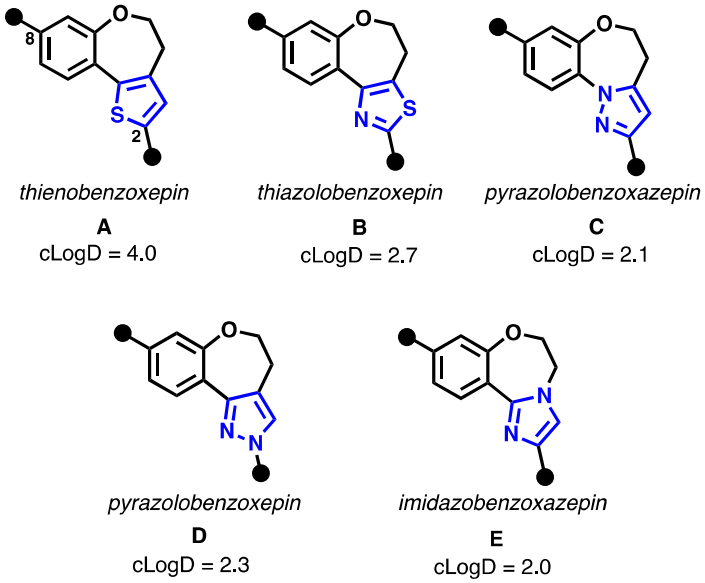

Figure 2. Scaffold replacements to reduce lipophilic nature of thiazolobenzoxepin **B** (cLogD values are given for analogs terminated by methyl groups).

Based on this singular factor alone, the imidazobenzoxazepin (**E**) may be expected to have decreased unbound clearance and improved solubility. We targeted analogs within the imidazobenzoxepin scaffold that were previously determined to be optimal for the thienobenzoxepin (**A**) and thiazolobenzoxepin (**B**) series based upon prior structural knowledge.[11,12] In particular, we selected to retain the pyrazole substituent at the 8-position and the triazole at the 2-position (based on the thienobenzoxepin numbering, Figure 2) because we were content with the benefits that they provided with regards to potency, selectivity and pharmacokinetics.

Results and Discussion

Chemistry

The preparation of imidazobenzoxazepin compounds was carried out in a similar vein to the strategies described previously.[18] One distinct feature of this scaffold is the presence of the bridgehead nitrogen in the fused tricycle. To fashion the tricyclic core, we subjected commercially available salicaldehyde **3** to a condensation reaction with glyoxal and two equivalents of ammonia to provide **4** (Scheme 1). Subsequently, **4** was subjected to 7-membered ring annulation with 1,2-dibromoethane in high dilution to minimize undesired bimolecular elimination (E2) by-product. The corresponding imidazobenzoxazepin tricycle (**5**) was then functionalized at the C-4 position of the imidazole ring employing a two-step sequence. We originally observed that electrophilic aromatic halogenation occurred preferentially at the C-5 at a rate faster than at the C-4 in line with previous reports.[19] Thus, use of at least two equivalents of *N*-iodosuccinimide provided the di-iodo intermediate **6** in good yield, and no further iodination was observed beyond the diiode. This compound was readily mono-deiodinated with a Grignard reagent, taking advantage of the heightened reactivity at C-5 to adjust the functionality to the desired bromoiodide **7**.[20]

Scheme 1. Synthetic route to the imidazobenzoxazepin bromoiodide core

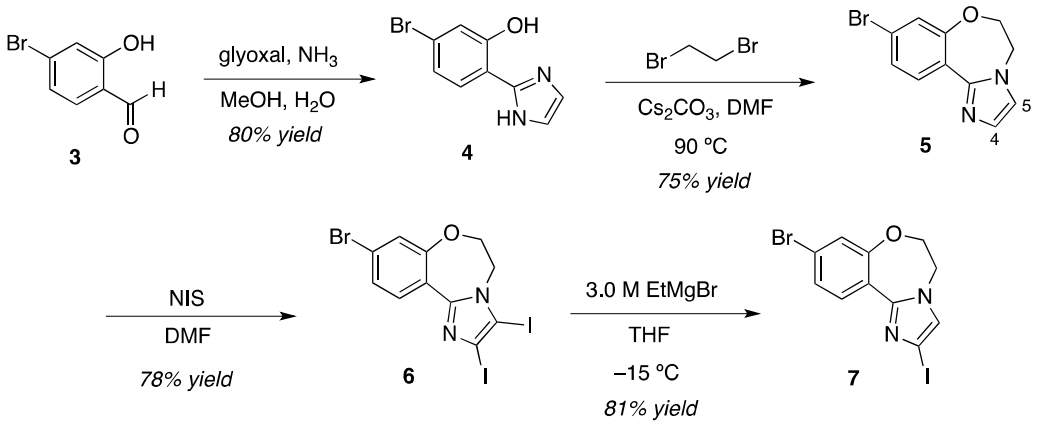

At this point, the synthesis of the various analogs diverged. The compounds were assembled by carbonylative amidation of bromoiodide **7** selectively at the iodide to generate the primary amide **8** (Scheme 2).[21] Regioselective triazole formation can be carried out with a variety of hydrazines as previously described.[18] Finally, reaction of the bromide with a diversity of pyrazole boronic acids or esters under Suzuki conditions provided the compounds (**11a-l**) described in this manuscript.

Scheme 2. Elaboration of bromoiodide **7** to PI3K inhibitors (**11a-l**).

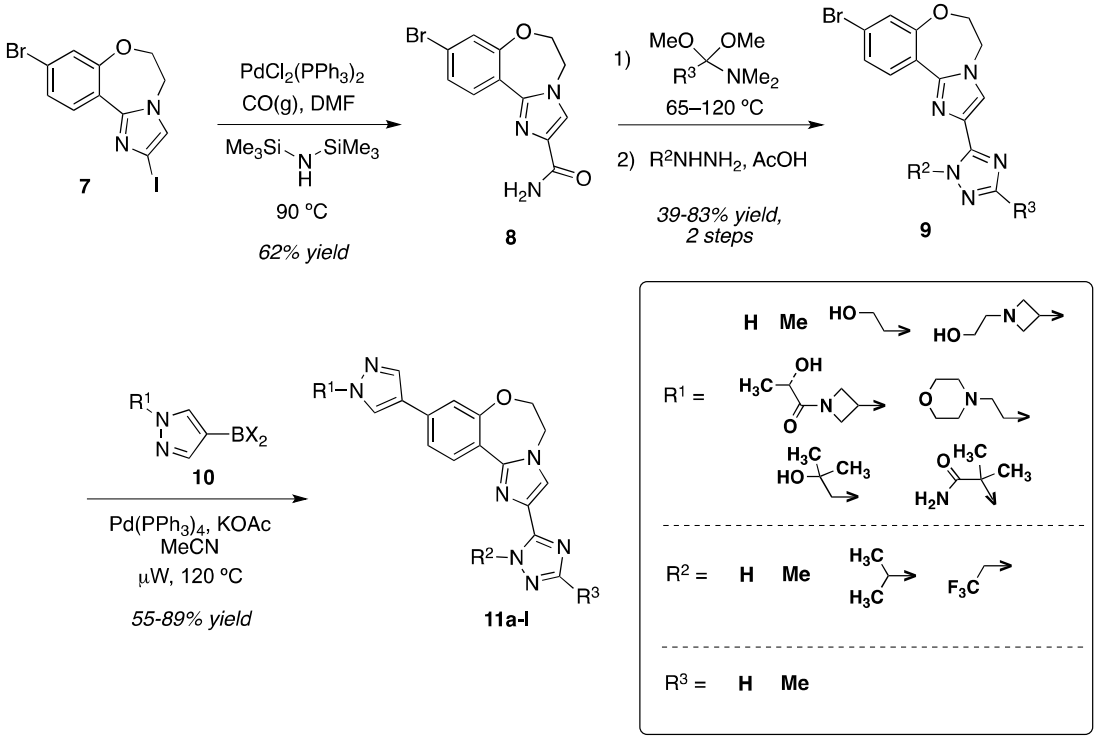

In vitro Activity

Our initial investigations began with measuring the effect that changing the groups on the pyrazole and triazole substituents had on PI3Kα biochemical potency, selectivity over PI3Kβ and cell-based activity (p-Akt and MCF7-neo/HER2 proliferation). In addition, the mouse liver microsomal intrinsic clearance (Cl_{int}) and kinetic solubility were also determined (Table 2). In general, it was noted that changes to the triazole substituents pointing towards the affinity pocket in PI3Kα, R^2 and R^3, had the greatest impact to potency

whereas the substituents on the pyrazole pointing out towards solvent, R^1, were used to tune PI3Kβ selectivity as well as physicochemical properties, particularly cLogD.[10,12] In the variations evaluated, careful effort was taken in the design process to avoid introduction of severe metabolic soft spots within the molecules.

Table 2 PI3Kα biochemical activity, β-sparing ratio, cellular activities and mouse liver microsome intrinsic clearance as a function of structural changes.[a]

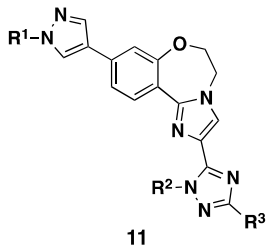

11

Compound	R^1	R^2	R^3	cLogD	PI3Kα K_i (nM)[b]	β/α[c]	p-Akt IC_{50} (nM)	MCF7-neo/HER2 prolif IC_{50} (μM)	MLM CL_{int} (mL/min/kg)[d]	Kinetic Solubility (μM)
11a	**H**		H	3.1	0.31	26x	n.t.[e]	0.218	550	<1.0
11b	**CH_3**		**CH_3**	3.3	0.29	20x	0.71	0.157	82.0	2.0
11c			**CH_3**	2.6	0.40	35x	4.5	0.138	68.1	2.1
11d		**H**	**CH_3**	1.6	21.1	33x	n.t.[e]	>10	n.d.	95.8
11e		**CH_3**	**CH_3**	1.8	2.8	35x	n.t.[e]	1.4	100	2.4
11f			**H**	2.5	0.17	39x	5.4	0.092	42.9	5.1
11g			**H**	2.5	<0.1	62x	2.9	0.066	28.0	7.6
11h	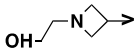		**CH_3**	2.0	0.11	83x	1.4	0.120	58.0	109
11i	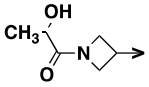		**CH_3**	2.3	0.34	43x	0.93	0.102	23.0	78.2
11j	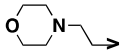		**CH_3**	2.8	0.30	58x	35	0.248	89.4	52.3
11k	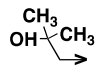		**H**	3.3	0.14	67x	9.4	0.081	44.3	12.4
11l	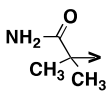		**CH_3**	2.5	0.29	31x	4.0	0.025	41.1	33.1

[a]See Table 1 for assay descriptions. [b]Ki values are an average of 3 independent experiments. Each value has a standard deviation of less than one geometric mean. [c]Ratio of PI3Kβ IC_{50} over PI3Kα apparent K_i, x = fold; [d]Compounds were incubated with mouse liver microsomes for 1 h and % remaining was determined by LC-MS/MS analysis. [e]Not tested, the compound was not evaluated in this assay.

We began our survey with the imidazobenzoxazepin **11a** bearing an isopropyl substituent on the triazole similar to the thiazolobenzoxepin **2**. Biochemical and cellular potencies were reasonable but intrinsic microsomal clearance was high at 550 ml/min/kg. This rate of metabolic clearance was not tolerable. A simple substitution with a 1-methyl group on the pyrazole near the solvent-exposed region of the ligand and a 3-methyl group on the triazole helped to significantly improve mouse liver microsome (MLM) clearance (**11b**). However, the kinetic solubility of 2 μM remained unacceptably low. Placement of a polar substituent such as a hydroxyethyl tail on the pyrazole near the solvent-exposed front pocket was effective in reducing cLogD to 2.6 for **11c** while maintaining good biochemical activity. This change was well tolerated and resulted in a slight improvement of cell-based potency and metabolic clearance. Further reduction of cLogD by removing the isopropyl substituent on the triazole altogether and replacing with either the less lipophilic *N*-H (**11d**) and *N*-methyl (**11e**) led to 50-fold and 5-fold loss in potency, respectively. Re-insertion of the isopropyl group and removal of the 3-methyl group resulted in a compound with increased potency and microsomal clearance (**11f** vs. **11c**). Further modifications to the triazole revealed that a 2,2,2-trifluoroethyl substituent in **11g** was an effective replacement of the isopropyl, with comparable biochemical and cellular activity. Metabolic clearance was also slightly improved with this replacement. Next, we investigated the substituents at the 1-position of the pyrazole to help improve kinetic solubility. As mentioned previously, this portion of the inhibitor extends toward solvent, so we reasoned that various groups would be tolerated in this region. Therefore, a number of polar groups at this position were evaluated with all of the analogs showing effective kinase inhibition with sub-nM activity against PI3Kα, good cell-based activity and kinetic solubility (**11h-j**). Finally, the tertiary alcohol (**11k**) and the α-quaternary amide (**11l**) pyrazole substituents were also evaluated. These latter compounds possessed a favorable balance of all of the properties that we optimized for: enzymatic and cellular activity, microsomal clearance and kinetic solubility. It is noteworthy that all the compounds described had desirable levels of selectivity over PI3Kβ, which was attributed to the pyrazole substitution that they shared in common.[10,12]

Pharmacokinetic properties

From the data gathered thus far, **11c**, **11k** and **11l** were selected for progression into in vivo pharmacokinetic (PK) profiling. A single dose of each compound was administered to adult female nude mice either intravenously at 1 mg/kg or orally at 25 mg/kg. The data for these three compounds are summarized in Table 3. When compared to the original thiazolobenzoxepin inhibitor **2**, the imidazobenzoxazepin inhibitors (**11c**, **11k** and **11l**) all showed improved anti-proliferative cellular activity in MCF7-neo/HER2 line (138, 81 and 25 nM, respectively). Additionally, in line with their low in vitro clearance, the mouse plasma clearance (CL_p) values were also low for these optimized compounds. More importantly, in each case both the unbound clearance (CL_u) and, correspondingly, the unbound oral exposure (AUC_u) were significantly (>10x) improved relative to thiazolobenzoxepin **2**. Compound **11l** provided the highest unbound exposure of the compounds tested (AUC_u = 42 μM•hr). Based on these results, we selected **11l** to evaluate in an in vivo tumor xenograft study in a head-to-head comparison with compound **1**.

Table 3. Cellular anti-proliferative activity and pharmacokinetic profiles of imidazobenzoxazepins (compounds **11c**, **11k** and **11l**) compared to thiazolobenzoxepin **2**.

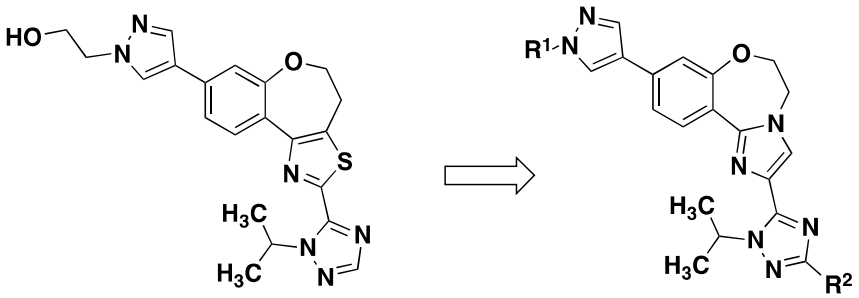

2 **11c, 11k** and **11l**

Compound	R_1	R_2	MCF7-neo/HER2 prolif IC_{50} (μM)	cLogD	% mouse PPB [a]	Mouse PK i.v., p.o. (1, 25 mg/kg) CL_p (mL/min/kg)	CL_u (mL/min/kg) [b]	AUC_{tot} (μM•h)	AUC_u (μM•h) [c]
2	--	--	0.195	3.8	99.8	9.5	4750	112	0.22
11c	HO	CH_3	0.138	2.6	98.2	1.5	83	291	5.2
11k	H_3C, HO, CH_3	H	0.081	3.3	98.3	4.8	282	156	2.7
11l	H_2N, O, H_3C, CH_3	CH_3	0.025	2.5	89.3	2.7	25	388	42

[a] % Plasma protein binding measured with equilibrium dialysis. [b] $CL_u = CL_p / f_u$. [c] $AUC_u = AUC_{tot} \times f_u$; f_u = (100 – %PPB) / 100.

In vivo Efficacy and Pharmacodynamics

The in vivo efficacy of compound **11l** was compared to compound **1** in the MCF7-neo/Her2 xenograft model grown in nude mice. Daily, oral administration of compound **1** at 45 mg/kg resulted in 69% tumor growth inhibition (TGI) when compared to vehicle treated mice (purple curve, Figure 3). Daily administration of compound **11l** orally at 1.4, 2.8, 5.8, 11.25, or 22.5 mg/kg resulted in dose-dependent increase in TGI (19%, 76%, 95%, 103%, and 123%, respectively) and tumor regressions when compared to vehicle treated mice. The increased potency and unbound concentration of compound **11l** resulted in comparable TGI (76%) to compound **1** (69%) at a dose that is approximately 16-fold lower (2.8 mg/kg versus 45 mg/kg). Treatment of

both compound **1** and **11l** were well tolerated with less than 10% body weight loss observed compared to vehicle controls (data not shown).

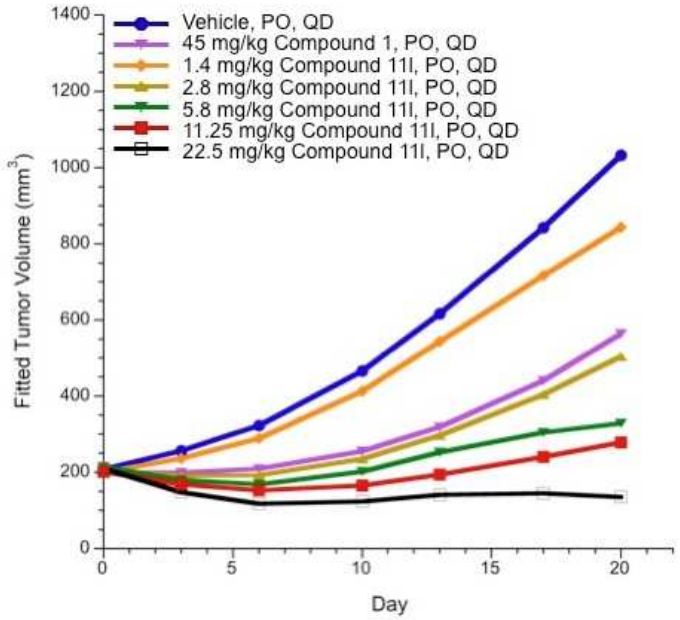

Figure 3 Dose-response curves of fitted tumor volumes in response to **1** and **11l** at the doses shown against MCF7-neo/HER2 xenografts in mice relative to vehicle (MCT; 0.5% methycellulose/0.2% Tween-80) after daily (QD) oral (PO) dosing for 20 days.

The relationship between pharmacokinetics (PK) and pharmacodynamics (PD) of compound **11l** relative to compound **1** was also investigated in the MCF7-neo/Her2 xenograft model (Figure 4). The phosphorylation levels of Akt in MCF7-neo/HER2 tumors, as well as plasma drug concentrations of both compounds, were evaluated 1 hour after a single dose of vehicle (MCT), compound **1** at 45 mg/kg or compound **11l** at 1.4, 2.8, 5.8, 11.25, or 22.5 mg/kg. Compound **1** resulted in 58% decrease of phosphorylation of Akt ($pAkt^{Ser473}$) levels while a 16-fold lower dose of compound **11l** at 2.8 mg/kg resulted in a similar decrease in Akt phosphorylation (59%). The comparable decreases in pAkt between these doses of compound **11l** and **1** is

likely due to similar unbound plasma drug concentrations that were achieved in mice after 1 hour of dosing (Figure 4).

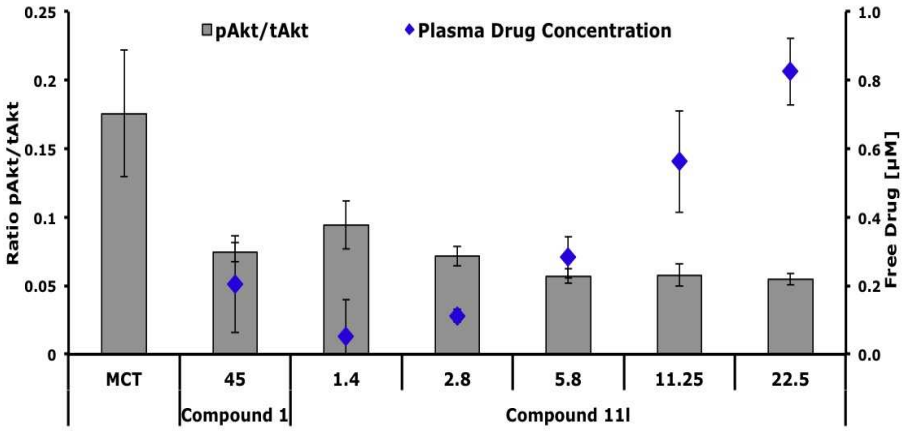

Figure 4) Quantification of pAkt^{Ser473} levels in MCF7-neo-Her2 tumor xenografts 1 hour after a single dose of MCT vehicle (0.5% methycellulose/0.2% Tween-80), compound **1** at 45 mg/kg or compound **11l** at 1.4, 2.8, 5.8, 11.125, or 22.5 mg/kg. Phosphorylated Akt (pAkt^{Ser473}) and total Akt (tAkt) levels were measured by Mesoscale Discovery assay and values are expressed as ratio of pAkt/tAkt. Error bars represent SEM for tumor xenograft samples from four different animals. Corresponding plasma free drug concentrations (closed diamonds) for each dose of compound **1** or compound **11l** are plotted on the right y-axis.

To better understand the differences in pharmacokinetic properties between thiazolobenzoxepin (e.g. **2**) and imidazobenzoxazepin (e.g. **11l**) inhibitors, it is necessary to consider the impact of reducing cLogD had on metabolic clearance. This analysis can be applied to all five scaffolds (**A**–**E**) previously introduced in Figure 2 in order to generalize the observation.

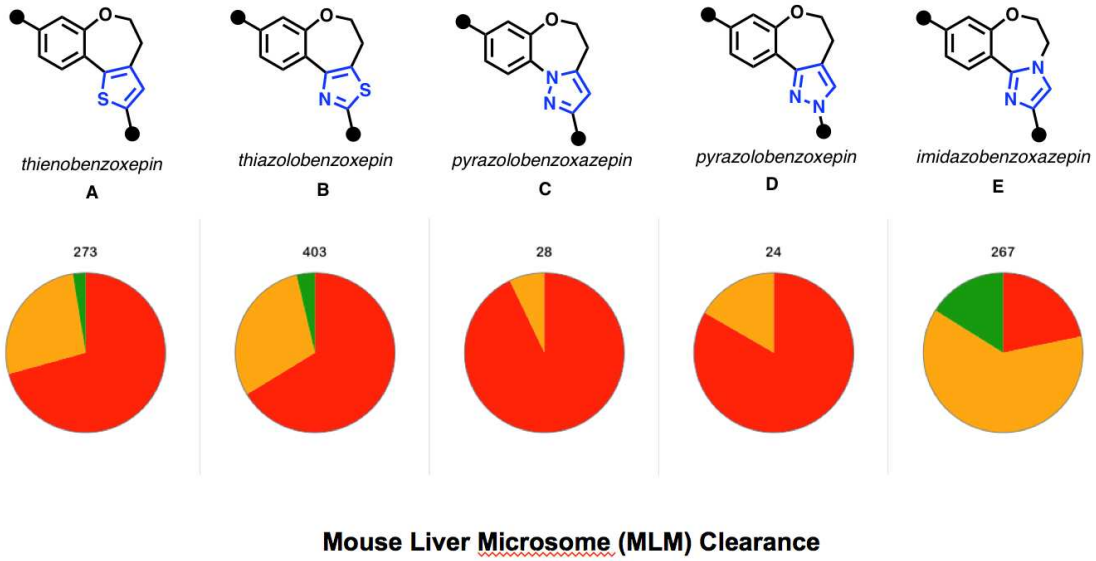

Figure 5. Pie charts of mouse liver microsomal clearance categories according to scaffold **A**–**E**. Numbers above individual pie charts correspond to sample size. Green = stable, <27 mL/min/kg; orange = moderate, 27-63 mL/min/kg; and red = high, >63 mL/min/kg.

When compounds from each of the sub-series were incubated with mouse liver microsomes (MLM), the imidazobenzoxepin (**E**) had the greatest ratio of compounds (>75%) measured to be in the moderate or low clearance category (CL_{hep} < 63 mL/min/kg). In contrast, the other scaffolds had more compounds fall in the high clearance category. This outcome can be attributed to two main factors: first, this series was the least lipophilic as determined by cLogD; secondly, and more important to our understanding, the oxidative potential of the α-methylene position vary depending on the adjacent heterocycles present in each core.[22] By blocking this particular metabolic soft spot, we can effectively lower clearance rate, all else being equal. In silico, the degree to which this oxidation could occur was determined using the computational program MetaSite® (Figure 6).[23] The program indicated that the preferred site of oxidation on the core was at this soft spot for the compounds analyzed (shaded spheres). The oxidation at this site was severe for thienobenzoxepin **A** and thiazolobenzoxepin **B**. To a lesser degree, pyrazolobenzoxazepin **C** and

pyrazolobenzoxepin **D** were also calculated to be mildly susceptible to oxidation. However, imidazobenzoxazepin **E** was calculated as not experiencing any such oxidation at this α-methylene position. One possible explanation for the attenuated reactivity at this site for **E** was that the nitrogen atom directly attached to the position in question was shielding it from cytochrome P450 enzymes. The polarization of this methylene group by the imidazole nitrogen can alter its susceptibility towards oxidation, thereby shifting metabolism on the molecule elsewhere. We confirmed that these calculations were relevant in a real setting by performing in vitro metabolite identification using compound **2** and **11l** following incubation with human hepatocytes. Indeed, the formation of a substantial amount of the oxidation product corresponding to **oxo-2** was observed after 4 h (Scheme 3a). Conversely, exposure of imidazobenzoxazepin **11l** to similar conditions yielded only minimal detectable quantity of the product corresponding to α-methylene oxidation (Scheme 3b).[24]

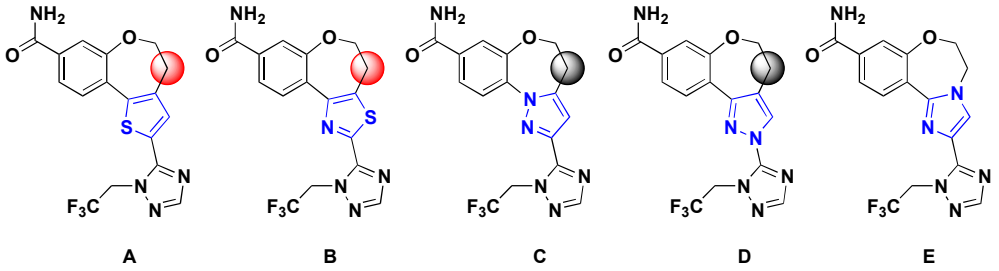

Figure 6. MetaSite® predictions for site of CYP-mediated oxidation of the α-methyl group adjacent to the heterocyclic subunit at the center of each scaffold **A**–**E**. Red spheres indicate severe magnitude of such oxidation while gray spheres indicate moderate oxidation.

Scheme 3. Thiazolobenzoxepin **2** was extensively converted to the oxidized product when incubated with human hepatocytes. The corresponding product is minimal when **11l** is subjected to similar conditions.

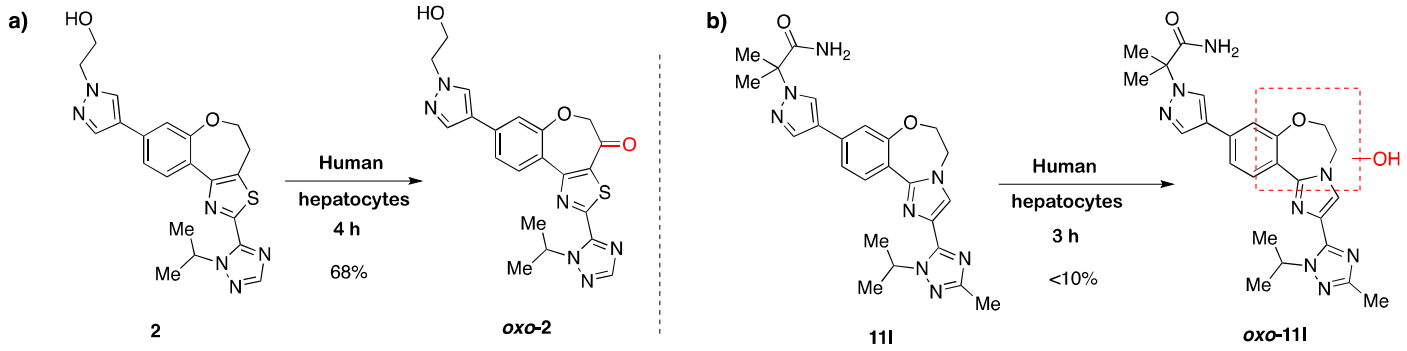

By masking a metabolic site, we managed to reduce both the in vivo clearance and (because we concomitantly increased free fraction) the unbound clearance as well. To confirm that the improvement to the unbound plasma clearance was general for the imidazobenzoxazepin (**E**) scaffold relative to the thiazolobenzoxepin (**B**), we plotted CL_u for ten matched-pair comparisons where compounds differed only by the composition of their central core, imidazole versus thiazole (Figure 7). In all cases evaluated, **E** consistently showed lower CL_u for each pair with direct analogs in both scaffolds. Ultimately, our strategy of transitioning to the imidazobenzoxazepin scaffold proved beneficial in generating well-behaved compounds that achieve high unbound exposures in vivo.

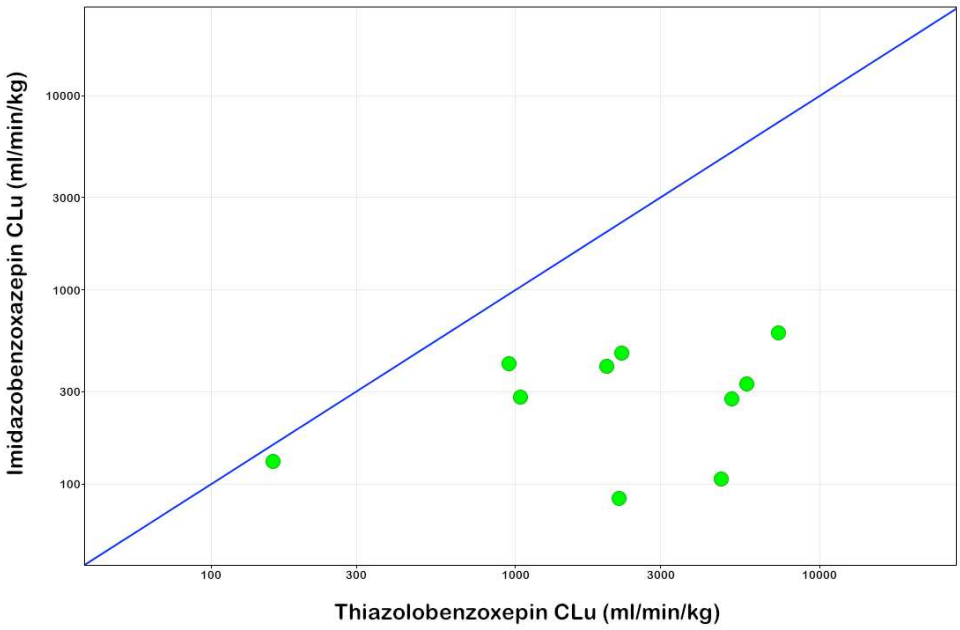

Figure 7. Two-dimensional plot of ten matched-pair comparisons with unbound clearance (CL_u) of imidazobenzoxazepins (**E**) on the *y*-axis and thiazolobenzoxepins (**B**) on the *x*-axis. The diagonal blue line represents the line of unity.

Therapeutic candidate profile

Consequently, compound **11l** was extensively characterized to determine if it met our criteria for a therapeutic candidate for use in clinical trials (Figure 8). Earlier, we established that it reached all expectations with regard to potency, PK/PD and efficacy in human xenograft mouse models. Selectivity against the broader kinome was also determined by screening against Invitrogen's SelectScreen panel of kinases. Out of 235 kinases that were screened with **11l** at 1 μM, we found that only 5 kinases were inhibited >50%: PI3K-C2 beta, PI3Kα, PI3Kδ, PI3Kγ and hVPS34 at 80.4%, 98.6%, 97.9%, 90.6% and 69.9%, respectively. Notably, PI3Kβ was not included in the panel of kinases screened. Measurement of IC_{50}s for potently inhibited kinases showed that we indeed maintained biochemical selectivity over the non-Class I PI3Ks, with IC_{50} for PI3K-C2 beta and hVPS34 measuring 292 nM and 374 nM, respectively. Compared to the 290 pM activity against PI3Kα, we achieve a 1000-fold selectivity against these potential off-targets. The

favorable pharmacokinetic profile evident in nude mouse was also achieved in Sprague–Dawley rats. We observed low clearance (CL_P = 1.8 ml/min/kg) and high oral bioavailability (F = 99%) consistent with in vitro experiments carried out in hepatocytes that suggested low metabolic clearance. Auspiciously, the clearance predicted by human hepatocytes is low, suggesting low plasma clearance could be achieved in vivo. After these and further analyses, which included toxicological and safety evaluation, we determined that **11l** had a satisfactory profile to progress into human clinical trials.[25]

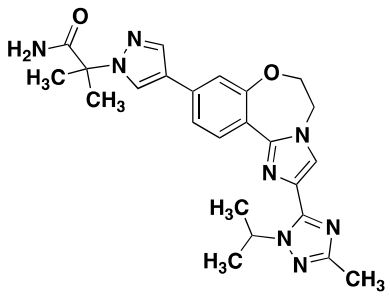

11l

Biochemical activity (nM):
K_i's: PI3Kα = 0.29
PI3Kβ = 9.1 (β/α = 31x)
PI3Kδ = 0.12
PI3Kγ = 0.97

Cell activity (μM):
IC_{50} (p-Akt: MCF7) = 0.004
IC_{50} (p-Akt: PC3) = 0.031

Proliferation (μM):
EC_{50} (MCF7) = 0.025
EC_{50} (PC3) = 0.571

Kinase selectivity:
<50% inhibition against 230 kinases @ 1 μM
(Complete Invitrogen kinase panel)

PIKK family selectivity (IC_{50}):
Class II (C2alpha/beta): >10 μM / 0.292 μM
Class III (hVPS34): 0.374 μM
Class IV (DNA-PK): >4.8 μM
mTor: K_i = 1.2 μM

Metabolic stability (Hepatocytes):
CL_{hep} (ml/min/kg):
Human / Mouse / Rat
3.2 5.2 11

In vivo pharmacokinetics:
Mouse: CL_P = 2.7 ml/min/kg; F = 100%
Rat: CL_P = 1.8 ml/min/kg; F = 99%

Plasma Protein Binding:
Human: 76% Rat: 98% Mouse: 89%

Figure 8. Preclinical candidate profile of PI3Kβ-sparing inhibitor **11l**.

Conclusions

In summary, we discovered a novel class of compounds for the inhibition of PI3K driven tumors. The key feature for optimization was improving unbound exposure (AUC_u) by reducing cLogD as a design parameter. This improvement had profound effects on tumor growth inhibition in vivo. Relative to a closely

related benzoxepin scaffold evaluated, the imidazobenzoxazepin had better tumor growth inhibition at even lower drug doses. In line with the free drug hypothesis, reducing the intrinsic plasma clearance (in this case, a result of removing metabolic soft spots) and increasing free exposure resulted in more efficacious drugs. This approach was essential because we had access to a substantial set of data for comparing direct analogs in several closely related scaffolds. As a result, we quickly settled on a suitable scaffold to optimize in order to achieve the desired profile. Our optimization efforts led to the identification of **11l** (or GDC-0032), currently undergoing clinical development for use in PI3K-related cancers.

EXPERIMENTAL SECTION

Computation.

Using MoKa Software (version 1.1.0, Molecular Discovery) and a custom pK_a model augmented with Roche internal data, logarithm of the acid dissociation constant of most basic center (cpK_{a_MB}), logarithm of the partition coefficient (clogP), and logarithm of the distribution coefficient at pH 7.4 (clogD) were calculated. Metabolic soft spots were predicted using MetaSite. The program calculates a probability of CYP-based metabolism at certain sites of a molecule by considering both accessibility of the atoms to the reactive heme and their reactivity in the appropriate reaction mechanism.[23] Accessibility was derived by comparing GRID-based fingerprint representations of a CYP450 binding site and a 3D structure of the substrate. Substrate reactivity was computed from a mixture of molecular orbital calculations and fragment recognition.

Chemistry. General Methods. All solvents and reagents were used as obtained. Reactions involving air or moisture sensitive reagents were carried out under nitrogen atmosphere. Microwave reactions were performed using CEM Discover and Biotage Initiator reactors. NMR spectra were recorded in a deuterated

solvent with a Bruker Avance 400- or 500-MHz NMR spectrometer, and referenced to trimethylsilane (TMS). Chemical shifts are expressed as δ units using TMS as the external standard (in NMR description, s = singlet, d = doublet, t = triplet, q = quartet, m = multiplet, and br = broad peak). All coupling constants (*J*) are reported in Hertz. Mass spectra were measured with a Finnigan SSQ710C spectrometer using an ESI source coupled to a Waters 600MS HPLC system operating in reverse mode with an X-bridge Phenyl column of dimensions 150 mm by 2.6 mm, with a 5 μm sized particles. Analytical purity was >95% unless stated otherwise. The following analytical method was used to determine chemical purity of final compounds unless otherwise stated: HPLC-Agilent 1200, water with 0.05% TFA, acetonitrile with 0.05% TFA, Agilent Zorbax SD-C18, 1.8 μM, 2.1x30 mm, 40 ºC, 3-95% B in 8.5 min, 95% in 2.5 min, 400 μL/min, 220 nm and 254 nm, equipped with Agilent quadrupole 6140, ESI positive, 110-800 amu.

Ethyl 4-(3-bromophenoxy)butanoate (12)

Solid 3-bromophenol (10.0 g, 58 mmol) was added portion wise to a stirred suspension of K_2CO_3 in acetone (100 mL) at room temperature. Sodium iodide (NaI, 1.0 g) was added, followed by ethyl-4-bromobutyrate (9.2 mL, 64 mmol). The reaction mixture was heated at 80 ˚C overnight, cooled to room temperature, diluted with water and extracted with ethyl acetate to give ethyl 4-(3-bromophenoxy)butanoate (**12**).

4-(3-bromophenoxy)butanoic acid (13)

Ethyl 4-(3-bromophenoxy)butanoate (**12**) was taken up in 100 mL THF and 50 mL water and treated with lithium hydroxide LiOH (hydrate, 4.9 g). The whole was heated at 50 ˚C for 2 days. The mixture was cooled to room temperature and acidified to pH 1 with 2N HCl. The aqueous was extracted with

ethylacetate. The combined organics were washed with brine and dried over sodium sulfate to give crude 4-(3-Bromophenoxy)butanoic acid (**13**) as a sticky solid. ^{1}H NMR (DMSO-d_6, 500 MHz) 7.24 (m, 1H), 7.13 (m, 1H), 7.11 (m, 1H), 6.95 (m, 1H), 3.99 (m, 2H), 2.37 (m, 2H), 1.94 (m, 2H).

8-bromo-3,4-dihydrobenzo[b]oxepin-5(2H)-one (14)

To a stirred suspension of polyphosphoric acid (PPA, ca. 60 g) and celite (ca. 40 g) in 100 mL toluene was added crude 4-(3-bromophenoxy)butanoic acid (**13**) (ca. 58 mmol) in one portion, 10 mL toluene rinse. The resultant suspension was heated at 110 ^{o}C for 5 hr. The toluene was decanted through a plug of celite and the remaining slurry was washed repeatedly with toluene and ethylacetate. The eluent was concentrated and purified by flash column chromatography (4:1 hex:EtOAc) to give 8-bromo-3,4-dihydrobenzo[b]oxepin-5(2H)-one (7 g, ca. 50% yield). ^{1}H NMR (DMSO-d_6, 500 MHz) 7.55 (d, J = 8.5 Hz, 1H), 7.37 (d, J = 1.5 Hz, 1H), 7.35 (dd, J = 8.5, 1.5 Hz, 1H), 4.24 (t, J = 6.5 Hz, 2H), 2.79 (t, J = 7.0 Hz, 2H), 2.14 (m, 2H).

4,8-dibromo-3,4-dihydrobenzo[b]oxepin-5(2H)-one (15)

To a stirred solution of 8-bromo-3,4-dihydro-2*H*-benzo[b]oxepin-5-one (3.10 g; 12.8 mmol) in Et_2O at 0 °C was added Br_2 (625 µl; 12.2 mmol) and the reaction mixture was allowed to warm to r.t. over 2 h. Volatiles were evaporated and the residue purified by flash column chromatography (0-20% EtOAc in hexanes) to give 4,8-dibromo-3,4-dihydrobenzo[b]oxepin-5(2H)-one (**15**) as a colorless solid (4.0 g, 96% yield). ^{1}H NMR (400 MHz, $CDCl_3$) δ 7.18-7.21 (m, 2H), 7.55 (d, J = 8.0, 1H), 4.87 (app. t, J = 5.2, 2H), 4.33-4.39 (m, 1H), 4.09-4.16 (m, 1H), 2.78-2.91 (m, 1H), 2.40-2.49 (m, 1H).

8-Bromo-4,5-dihydro-6-oxa-3-thia-1-aza-benzo[e]azulene-2-carboxylic acid ethyl ester (16)

To a stirred solution of 4,8-dibromo-3,4-dihydrobenzo[b]oxepin-5(2H)-one (2.17 g; 6.8 mmol) in EtOH (70 ml) was added ethyl thiooxamate (2.72 g; 20.4 mmol) and the reaction mixture was heated at reflux temperature over 4 d. The reaction mixture was concentrated and the residue purified by flash column chromatography (0-20% EtOAc in hexanes) to give 8-Bromo-4,5-dihydro-6-oxa-3-thia-1-aza-benzo[e]azulene-2-carboxylic acid ethyl ester (**16**) as a yellow solid (1.08 g, 45% yield). ^{1}H NMR (400 MHz, $CDCl_3$) δ 8.36 (d, J = 8.4, 1H), 7.16-7,22 (m, 2H), 4.42 (q, J = 7.2, 2H), 4.31 (app. t, J = 5.2, 2H), 3.32 (app. t, J = 5.2, 2H), 1.38 (t, J = 7.2, 3H).

8-Bromo-4,5-dihydro-6-oxa-3-thia-1-aza-benzo[e]azulene-2-carboxylic acid (17)

To a stirred solution of 8-Bromo-4,5-dihydro-6-oxa-3-thia-1-aza-benzo[e]azulene-2-carboxylic acid ethyl ester in THF (10 ml) and MeOH (5 ml) was added a solution of NaOH (117 mg, 2.9 mmol) in water (2 ml). The reaction mixture was stirred at room temperature for 2 h upon which time it was acidified with 2 M HCl. The aqueous was extracted with CH_2Cl_2 and the combined organics dried ($MgSO_4$) and concentrated to give 8-Bromo-4,5-dihydro-6-oxa-3-thia-1-aza-benzo[e]azulene-2-carboxylic acid as a colorless solid (396 mg; 83%). ^{1}H NMR (400 MHz, $CDCl_3$) δ 8.22 (d, J = 8.4, 1H), 7.19-7.24 (m, 2H), 4.33 (t, J = 5.2, 2H), 3.36 (t, J = 5.2, 2H).

2-{4-[2-(2-Isopropyl-2H-[1,2,4]triazol-3-yl)-4,5-dihydro-6-oxa-3-thia-1-aza-benzo[e]azulen-8-yl]-pyrazol-1-yl}-ethanol (2)[12]

8-bromo-2-(2-isopropyl-2H-[1,2,4]triazol-3-yl)-4,5-dihydro-6-oxa-3-thia-1-aza-benzo[e]azulene (**17**) was reacted with ethyl 2-(4-(4,4,5,5-tetramethyl-1,3,2-dioxaborolan-2-yl)-1H-pyrazol-1-yl)acetate under typical Suzuki coupling conditions (*vide infra*) to give {4-[2-(2-Isopropyl-2H-[1,2,4]triazol-3-yl)-4,5-dihydro-6-oxa-3-thia-1-aza-benzo[e]azulen-8-yl]-pyrazol-1-yl}-acetic acid ethyl ester as a colorless solid. In a separate

preparation, a solution of {4-[2-(2-Isopropyl-2H-[1,2,4]triazol-3-yl)-4,5-dihydro-6-oxa-3-thia-1-aza-benzo[e]azulen-8-yl]-pyrazol-1-yl}-acetic acid ethyl ester in THF (200 mL) was cooled to 0 ^{o}C and treated drop wise with a solution of 1 M $LiAlH_4$ (in THF, 23 mL, 23 mmol, 2.5 eq). After 1 h, LC/MS indicated consumption of starting material. A solution of saturated sodium sulfate was added slowly until H_2 evolution ceased. ~30 g of solid magnesium sulfate was added and the whole was stirred for 20 min. Filtration over celite (EtOAc and DCM) followed by concentration of the filtrate gave a crude residue that was purified by rp-HPLC to give 1.4 g of **2** (43%). ^{1}H NMR (500 MHz, DMSO-d_6) δ 8.36 – 8.29 (m, 1H), 8.23 (s, 1H), 8.11 (d, *J* = 1.7 Hz, 1H), 7.97 (s, 1H), 7.44 (dd, *J* = 8.3, 1.8 Hz, 1H), 7.31 (d, *J* = 1.8 Hz, 1H), 5.84 (hept, *J* = 6.6 Hz, 1H), 4.95 (t, *J* = 5.3 Hz, 1H), 4.39 (t, *J* = 5.0 Hz, 2H), 4.16 (dd, *J* = 7.1, 4.3 Hz, 2H), 3.77 (q, *J* = 5.6 Hz, 2H), 3.44 (t, *J* = 5.1 Hz, 2H), 1.56 (d, *J* = 6.5 Hz, 6H). ^{13}C NMR (126 MHz, DMSO-d_6) δ 158.36, 152.50, 150.65, 148.05, 148.01, 145.40, 136.37, 134.51, 134.48, 133.85, 130.12, 128.05, 121.46, 120.50, 119.83, 116.65, 68.70, 59.94, 54.25, 51.58, 40.06, 39.97, 39.90, 39.80, 39.73, 39.63, 39.60, 39.47, 39.39, 39.30, 39.13, 38.97, 29.60, 22.02, 21.99. HRMS (ESI+): m/z ($M+Na^+$) calcd: 445.1423, found: 445.1518. Melting point: 180 ºC.

5-bromo-2-(1H-imidazol-2-yl)phenol (4)

4-Bromo-2-hydroxybenzaldehyde (1.0 g, 5 mmol), 40% aqueous solution of ethanedial (3.6 g, 24.9 mmol) and 50% aqueous ammonia (2.5 g) in methanol (20 mL) was stirred for 2 h or longer until the reaction is completed as determined by TLC. The solvent was removed under vacuum pressure and the residue was partitioned between EtOAc and water. The mixture was then filtered to remove the precipitate. The solution pH was adjusted to 5-6 by careful addition of 1 N HCl. The aqueous layer was extracted with EtOAc three times. The combined organic portions were washed with water, brine and dried over $MgSO_4$. The resulting residue was purified by ISCO chromatography (30% EtOAc/DCM) to provide 0.9 g (80% yield) of 5-bromo-

2-(1H-imidazol-2-yl)phenol (**4**) as a yellow solid. ^{1}H NMR (300 MHz, DMSO-d_6) δ 11.13 (bs, 1H), 10.23 (s, 1H), 7.57 (d, *J* = 8.3 Hz, 1H), 7.21 (d, *J* = 1.8 Hz, 1H), 7.18 – 7.09 (m, 1H), 3.35 (bs, 1H).

9-bromo-5,6-dihydrobenzo[f]imidazo[1,2-d][1,4]oxazepine (5)

A mixture of 5-bromo-2-(1H-imidazol-2-yl)phenol (0.9 g, 4 mmol), 1,2-dibromoethane (1.3 mL, 15 mmol) and cesium carbonate (4.9 g, 15 mmol) in DMF (20 mL) was heated to 90 ^{0}C for 12 h. The mixture was partitioned between water and EtOAc. The organic layer was separated, washed with water, brine and dried over $MgSO_4$. Concentrated in vacuo to yield the pure 9-bromo-5,6-dihydrobenzo[f]imidazo[1,2-d][1,4]oxazepine, 0.8 g (75% yield) (**5**). ^{1}H NMR (300 MHz, $CDCl_3$) δ 8.41 (d, *J* = 8.6 Hz, 1H), 7.31 – 7.21 (m, 3H), 7.19 (d, *J* = 1.1 Hz, 1H), 7.01 (d, *J* = 1.0 Hz, 1H), 4.59 – 4.26 (m, 4H).

9-bromo-2,3-diiodo-5,6-dihydrobenzo[f]imidazo[1,2-d][1,4]oxazepine (6)

A mixture of 9-bromo-5,6-dihydrobenzo[f]imidazo[1,2-d][1,4]oxazepine (0.8 g, 3 mmol) and *N*-iodosuccinimide (1.87 g, 8.3 mmol) in DMF was stirred at room temperature for 48 h. The mixture was diluted with EtOAc, washed with 5% sodium bicarbonate solution, 10% sodium thiosulfate, water and brine and the organic layer was dried over $MgSO_4$ and concentrated to a solid residue. Purification by ISCO chromatography (30% EtOAc/heptane) yielded 1.2 g (78% yield) of 9-bromo-2,3-diiodo-5,6-dihydrobenzo[f]imidazo[1,2-d][1,4]oxazepine (**6**). ^{1}H NMR (300 MHz, DMSO-d_6) δ 8.19 (d, *J* = 8.6 Hz, 1H), 7.35 – 7.18 (m, 2H), 4.58 – 4.24 (m, 4H).

9-bromo-2-iodo-5,6-dihydrobenzo[f]imidazo[1,2-d][1,4]oxazepine (7)

A 3.0 M solution of ethylmagnesium bromide in diethyl ether (1.1 mL, 3.3 mmol) was added dropwise to a cold suspension of 9-bromo-2,3-diiodo-5,6-dihydrobenzo[f]imidazo[1,2-d][1,4]oxazepine (1.1 g, 2.2 mmol) in THF at –15 □C. The mixture was stirred at cold temperature and monitored by LC/MS. After 1 h, full conversion was observed and the reaction was poured into saturated ammonium chloride and extracted with EtOAc. The organic extracts were washed with water, brine and dried over $MgSO_4$ and concentrated in vacuo. The crude residue was purified by flash column chromatography (EtOAc) to provide 0.7 g (81% yield) 9-bromo-2-iodo-5,6-dihydrobenzo[f]imidazo[1,2-d][1,4]oxazepine (**7**) as a white solid. ^{1}H NMR (300 MHz, DMSO-d_6) δ 8.22 (d, *J* = 8.5 Hz, 1H), 7.55 (s, 1H), 7.27 (dt, *J* = 5.5, 1.9 Hz, 2H), 4.43 (q, *J* = 6.1 Hz, 4H). ^{13}C NMR (75 MHz, DMSO) δ 155.9, 145.1, 131.4, 128.8, 125.8, 123.4, 122.4, 117.4, 83.7, 69.0, 49.8.

9-bromo-5,6-dihydrobenzo[f]imidazo[1,2-d][1,4]oxazepine-2-carboxamide (8)

9-bromo-2-iodo-5,6-dihydrobenzo[f]imidazo[1,2-d][1,4]oxazepine (1.5 g, 3.8 mmol) was placed in a 100-mL rbf and bis(triphenylphosphine) palladium(II) chloride (142 mg, 0.202 mmol) was added followed by DMF (45 mL) and hexamethyldisilazane (4.34 mL, 20.6 mmol). The entire solution was purged with a CO balloon and sealed with the CO balloon attached. The reaction flask was heated at 70 °C for 2 h. LC/MS indicated clean conversion at the end of this period. Cooled to room temperature and poured into 1 N HCl (30 mL). Stirred for 5 min and neutralized with sat. aq. $NaHCO_3$ soln. Extracted three times with EtOAc, dried over $MgSO_4$, filtered and concentrated in vacuo. Triturated with IPA and the solids were collected after filtration and EtOAc wash. This provided 734 mg (62% yield) of 9-bromo-5,6-dihydrobenzo[f]imidazo[1,2-d][1,4]oxazepine-2-carboxamide (**8**) as a tan solid. ^{1}H NMR (400 MHz, $CDCl_3$) δ 8.36 (d, *J* = 8.5, 1H), 7.63 (s, 1H), 7.24 (dd, *J* = 7.2, 4.2, 1H), 7.09 – 6.99 (m, 1H), 4.51 – 4.36 (m, 4H). LC/MS (ESI+): m/z 310 (M+H).

9-bromo-2-(1-isopropyl-1H-1,2,4-triazol-5-yl)-5,6-dihydrobenzo[f]imidazo[1,2-d][1,4]oxazepine (9a)

9-bromo-5,6-dihydrobenzo[f]imidazo[1,2-d][1,4]oxazepine-2-carboxamide (4.93 g, 16.0 mmol, a separate lot from previously) was taken up in 1,1-dimethoxy-*N*,*N*-dimethylmethanamine (25 mL, 0.18 mol) and 1,2-dimethoxyethane (66.5 mL, 0.640 mol). The heterogeneous mixture was stirred very vigorously and heated at 65 °C for 1 h. LC/MS showed complete consumption of starting material at the end of this period. The reaction mixture was concentrated in vacuo and carried on to the subsequent reaction with no further purification steps applied. The crude product from the previous reaction (5.8 g, 16.0 mmol) was suspended in glacial acetic acid (53.2 mL) and isopropylhydrazine hydrochloride (4.36 g, 39.4 mmol) was added. The mixture was heated at 100 °C for 2 h. The reaction vessel was cooled to room temp and the solvent was removed in vacuo. The resultant residue was dry loaded onto silica gel and purified by ISCO chromatography (120 g column, 100% EtOAc). Totally, 2.3 g (39% yield) of 9-bromo-2-(1-isopropyl-1H-1,2,4-triazol-5-yl)-5,6-dihydrobenzo[f]imidazo[1,2-d][1,4]oxazepine (**9a**) was isolated over the two steps. ^{1}H NMR (400 MHz, DMSO-d_6) δ 8.34 (d, *J* = 8.6, 1H), 7.95 (s, 1H), 7.91 (s, 1H), 7.36 (dd, *J* = 8.7, 2.0, 1H), 7.30 (d, *J* = 2.0, 1H), 5.85 (dt, *J* = 13.3, 6.6, 1H), 4.55 (d, *J* = 15.5, 4H), 1.48 (d, *J* = 6.6, 6H). LC/MS (ESI+): m/z 376 (M+H).

9-bromo-2-(1-(2,2,2-trifluoroethyl)-1H-1,2,4-triazol-5-yl)-5,6-dihydrobenzo[f]imidazo[1,2-d][1,4]oxazepine (9b)

Following the procedure described above, 9-bromo-5,6-dihydrobenzo[f]imidazo[1,2-d][1,4]oxazepine-2-carboxamide and (2,2,2-trifluoroethyl)hydrazine were reacted to give 9-bromo-2-(1-(2,2,2-trifluoroethyl)-1H-1,2,4-triazol-5-yl)-5,6-dihydrobenzo[f]imidazo[1,2-d][1,4]oxazepine (**9b**). ^{1}H NMR (400 MHz, DMSO-d_6) δ 8.28 (t, *J* = 21.9, 1H), 8.11 (t, *J* = 7.9, 2H), 7.51-7.35 (m, 1H), 7.32 (d, *J* = 2.0, 1H), 5.88 (q, *J* = 8.8, 2H), 4.76-4.29 (m, 4H). LC/MS (ESI+): m/z 413.9 (M+H).

9-bromo-2-(1-isopropyl-3-methyl-1H-1,2,4-triazol-5-yl)-5,6-dihydrobenzo[f]imidazo[1,2-d][1,4]oxazepine (9c)

9-bromo-5,6-dihydrobenzo[f]imidazo[1,2-d][1,4]oxazepine-2-carboxamide (5.1 g, 16 mmol) was taken up in toluene (100 mL) and treated with dimethylacetamide-dimethylacetal (26.5 mL, 178 mmol). This mixture was heated 2 h at 120 °C in a sealed vessel. LC/MS indicated complete consumption of starting material and formation of the acylamidine intermediate together with the hydrolysis by-product (40:60 mixture). This crude mixture was concentrated in vacuo to a yellow solid and combined with isopropylhydrazine hydrochloride (3.59 g, 32.4 mmol) in Acetic acid (50 mL) and heated at 95 °C for 1 h. The reaction was observed to be completed as determined by LC/MS. The reaction vessel was subsequently cooled to room temp and the volatiles were evaporated. The solid was dry-loaded onto an ISCO column and purified (120 g column, 10% MeOH/EtOAc) by flash column chromatography. This provided 5.9 g (95% yield) of 9-bromo-2-(1-isopropyl-3-methyl-1H-1,2,4-triazol-5-yl)-5,6-dihydrobenzo[f]imidazo[1,2-d][1,4]oxazepine (**9c**) as a tan-colored solid. ^{1}H NMR (400 MHz, $CDCl_3$) δ 8.38 (d, *J* = 8.6, 1H), 7.63 (s, 1H), 7.31 – 7.20 (m, 5H), 5.94 – 5.76 (m, 1H), 5.30 (s, 1H), 4.46 (ddd, *J* = 7.9, 6.2, 3.6, 4H), 2.41 (s, 3H), 1.67 – 1.45 (m, 7H).

1-[2-(Tetrahydro-pyran-2-yloxy)-ethyl]-4-(4,4,5,5-tetramethyl-[1,3,2]dioxaborolan-2-yl)-1H-pyrazole (10f)

To a solution of 4-pyrazole boronic acid pinacol ester (2.0 g, 10.3 mmol) in anhydrous DMF (20 mL) was added cesium carbonate (4.03 g, 12.4 mmol) and the mixture stirred at RT for 10 minutes. 2-(2-Bromoethoxy)tetrahydro-2H-pyran (1.87 mL, 12.4 mmol) was added in two portions and the mixture was heated to 70°C. After heating for 18 hours the mixture was allowed to cool to RT and partitioned between water (100 mL) and EtOAc (100 mL). The aqueous layer was washed with EtOAc (3 x 20 mL) and the combined organic layers washed with water (3 x 100 mL) followed by brine, dried (Na_2SO_4) and concentrated *in vacuo*. The resultant residue was purified by flash chromatography (SiO_2, gradient 0-100 % EtOAc in cyclohexane) to afford the title compound (2.15 g, 65 %). LC/MS: R_T = 3.97 min, $[M+Na]^+$ = 345.

2-Methyl-1-[4-(4,4,5,5-tetramethyl-[1,3,2]dioxaborolan-2-yl)-pyrazol-1-yl]-propan-2-ol (10l)

To a solution of 4-(4,4,5,5-tetramethyl-[1,3,2]dioxaborolan-2-yl)-1H-pyrazole (500 mg, 2.58 mmol) in 2,2-dimethyl-oxirane (3 mL) was added cesium carbonate (130 mg, 0.40 mmol). The reaction was heated at 120 °C for 30 minutes using microwave irradiation. The reaction was cooled then filtered through a plug of cotton wool, flushing with DCM. The filtrate was concentrated *in vacuo* giving 2-Methyl-1-[4-(4,4,5,5-tetramethyl-[1,3,2]dioxaborolan-2-yl)-pyrazol-1-yl]-propan-2-ol as a beige solid (620 mg, 90%). ^{1}H NMR (400 MHz, $CDCl_3$) δ 7.82 (1 H, d, J = 0.65 Hz), 7.69 (1 H, s), 4.07 (2 H, s), 1.32 (12 H, s), 1.15 (6 H, s). One exchangeable proton was not detectable.

General procedure for Suzuki coupling of 8-bromo precursors:

2-{4-[2-(2-Isopropyl-2H-[1,2,4]triazol-3-yl)-4,5-dihydro-6-oxa-1,3a-diaza-benzo[e]azulen-8-yl]-pyrazol-1-yl}-ethanol (11f)

To a 10-mL microwave was added 9-bromo-2-(1-isopropyl-1H-1,2,4-triazol-5-yl)-5,6-dihydrobenzo[f]imidazo[1,2-d][1,4]oxazepin (**9a**) (0.210 g, 0.56 mmol) and potassium acetate (0.17 g, 1.68 mmol), MeCN (1 mL) and water (2 mL). The mixture was thoroughly purged with N_2. A solution of 1-(2-(tetrahydro-2H-pyran-2-yloxy)ethyl)-4-(4,4,5,5-tetramethyl-1,3,2-dioxaborolan-2-yl)-1H-pyrazole (**10f**) (0.271 g, 0.84 mmol) in MeCN (1 mL) was added, followed by tetrakis(triphenylphosphine) palladium (65 mg, 0.056 mmol) and the vial was sealed immediately. The mixture was irradiated with microwave at 120 ºC for 20 mins. Complete conversion was observed by LC/MS (a small amount of des-THP product was also evident). The reaction mixture was diluted with EtOAc and water and extracted three times with EtOAc. The organic phases were combined, dried with $MgSO_4$ and concentrated. The residue was purified using ISCO

chromatography eluting with 10% MeOH/EtOAc, which gave 170 mg, 0.35 mmol (62% yield) of a white foaming solid. This material was directly dissolved in DCM (2 mL) and treated with 4 M hydrogen chloride in 1,4-dioxane (0.35 mL). A white precipitate developed during the addition. The reaction was stirred at room temperature for 1 h, concentrated to dryness and dissolved in DMF/H_2O. The mixture was purified by rp-HPLC to provide 105 mg (74% yield) of 2-{4-[2-(2-isopropyl-2H-[1,2,4]triazol-3-yl)-4,5-dihydro-6-oxa-1,3a-diaza-benzo[e]azulen-8-yl]-pyrazol-1-yl}-ethanol (**11f**) as a white, partially crystalline solid. ^{1}H NMR (500 MHz, DMSO-d_6) δ 8.38 (d, *J* = 8.5 Hz, 1H), 8.24 (s, 1H), 7.97 (s, 1H), 7.92 (d, *J* = 1.9 Hz, 2H), 7.39 (dd, *J* = 8.3, 1.8 Hz, 1H), 7.28 (t, *J* = 1.9 Hz, 1H), 5.91 (hept, *J* = 6.6 Hz, 1H), 4.95 (t, *J* = 5.3 Hz, 1H), 4.53 (q, *J* = 5.9 Hz, 4H), 4.16 (t, *J* = 5.6 Hz, 2H), 3.77 (q, *J* = 5.5 Hz, 2H), 1.50 (d, *J* = 6.6 Hz, 6H). ^{13}C NMR (126 MHz, DMSO-d_6) δ 155.88, 150.18, 147.10, 144.05, 136.45, 134.64, 130.14, 130.00, 128.18, 123.77, 120.32, 119.21, 116.00, 115.15, 68.31, 59.93, 54.27, 50.24, 49.69, 40.06, 39.97, 39.90, 39.80, 39.73, 39.63, 39.62, 39.47, 39.40, 39.30, 39.13, 38.97, 22.32. HRMS (ESI+): m/z ($M+H^+$) calcd: 406.1991, found: 406.1972. Melting point: 216 ºC.

The following nine compounds were prepared analogously to **11f** by replacement with the corresponding organoboron (**10**) coupling partner (yields 55-89%):

2-(2-Isopropyl-5-methyl-2H-[1,2,4]triazol-3-yl)-8-(1-methyl-1H-pyrazol-4-yl)-4,5-dihydro-6-oxa-1,3a-diaza-benzo[e]azulene (11b)

^{1}H NMR (500 MHz, DMSO-d_6) δ 8.36 (d, *J* = 8.3 Hz, 1H), 8.22 (s, 1H), 7.94 (s, 1H), 7.88 (s, 1H), 7.37 (dd, *J* = 8.5, 1.7 Hz, 1H), 7.26 (d, *J* = 1.8 Hz, 1H), 5.93 – 5.76 (m, 1H), 4.57 – 4.44 (m, 4H), 3.87 (s, 3H), 2.26 (s, 3H), 1.47 (d, *J* = 6.7 Hz, 6H). ^{13}C NMR (126 MHz, DMSO-d_6) δ 158.24, 155.85, 147.29, 143.91, 136.40, 134.48, 130.28, 129.99, 128.33, 123.63, 120.70, 119.22, 116.03, 115.23, 99.49, 68.30, 49.88, 49.67, 40.06, 39.97, 39.90, 39.80, 39.74, 39.64, 39.61, 39.47, 39.40, 39.30, 39.13, 38.97, 38.72, 22.35, 22.31, 13.82. HRMS (ESI+): m/z ($M+Na^+$) calcd: 412.1862, found: 412.1892. Melting point: 230 ºC.

2-{4-[2-(2-Isopropyl-5-methyl-2H-[1,2,4]triazol-3-yl)-4,5-dihydro-6-oxa-1,3a-diaza-benzo[e]azulen-8-yl]-pyrazol-1-yl}-ethanol (11c)

^{1}H NMR (500 MHz, DMSO-d_6) δ 8.36 (d, *J* = 8.4 Hz, 1H), 8.23 (s, 1H), 7.96 (s, 1H), 7.88 (s, 1H), 7.39 (dd, *J* = 8.3, 1.8 Hz, 1H), 7.28 (d, *J* = 1.7 Hz, 1H), 5.95 – 5.76 (m, 1H), 4.95 (t, *J* = 5.3 Hz, 1H), 4.59 – 4.46 (m, 4H), 4.16 (t, *J* = 5.6 Hz, 2H), 3.77 (q, *J* = 5.5 Hz, 2H), 2.26 (s, 3H), 1.47 (d, *J* = 6.5 Hz, 6H). ^{13}C NMR (126 MHz, DMSO-d_6) δ 158.24, 155.86, 147.31, 143.93, 136.45, 134.61, 130.27, 129.98, 128.17, 123.63, 120.33, 119.21, 116.00, 115.19, 99.48, 68.30, 59.93, 54.27, 49.88, 49.68, 40.06, 39.97, 39.90, 39.80, 39.73, 39.63, 39.57, 39.47, 39.39, 39.30, 39.13, 38.97, 35.69, 22.35, 22.32, 13.82. HRMS (ESI+): m/z ($M+H^+$) calcd: 420.2148, found: 420.2141. Melting point: 247 ºC.

2-{4-[2-(5-Methyl-2H-[1,2,4]triazol-3-yl)-4,5-dihydro-6-oxa-1,3a-diaza-benzo[e]azulen-8-yl]-pyrazol-1-yl}-ethanol (11d)

^{1}H NMR (500 MHz, DMSO-d_6) δ 13.61 (d, *J* = 152.1 Hz, 1H), 8.43 (d, *J* = 20.4 Hz, 1H), 8.24 (s, 1H), 7.96 (s, 1H), 7.90 – 7.61 (m, 1H), 7.38 (d, *J* = 8.1 Hz, 1H), 7.27 (s, 1H), 4.95 (t, *J* = 5.2 Hz, 1H), 4.50 (s, 4H), 4.16 (dd, *J* = 7.1, 4.2 Hz, 2H), 3.77 (q, *J* = 5.4 Hz, 2H), 2.45 – 2.19 (m, 3H). ^{13}C NMR (126 MHz, DMSO-d_6) δ 159.48, 155.74, 152.58, 150.26, 144.19, 138.36, 136.38, 134.57, 134.07, 130.28, 130.10, 128.15, 121.70, 120.36, 119.03, 115.92, 115.26, 104.70, 68.41, 60.13, 59.91, 54.27, 53.79, 49.61, 49.51, 40.06, 39.96, 39.89, 39.80, 39.73, 39.63, 39.47, 39.40, 39.29, 39.13, 38.96, 13.71, 11.55. HRMS (ESI+): m/z ($M+H^+$) calcd: 378.1678, found: 378.1711. Melting point: 237 ºC.

2-{4-[2-(2,5-Dimethyl-2H-[1,2,4]triazol-3-yl)-4,5-dihydro-6-oxa-1,3a-diaza-benzo[e]azulen-8-yl]-pyrazol-1-yl}-ethanol (11e)

^{1}H NMR (500 MHz, DMSO-d_6) δ 8.40 (d, *J* = 8.5 Hz, 1H), 8.24 (s, 1H), 7.96 (s, 1H), 7.90 (s, 1H), 7.37 (dd, *J* = 8.5, 1.7 Hz, 1H), 7.28 (d, *J* = 1.8 Hz, 1H), 4.95 (t, *J* = 5.3 Hz, 1H), 4.60 – 4.42 (m, 4H), 4.22 (s, 3H), 4.16 (t, *J* = 5.6 Hz, 2H), 3.77 (q, *J* = 5.5 Hz, 2H), 2.24 (s, 3H). ^{13}C NMR (126 MHz, DMSO-d_6) δ 158.26, 155.85, 148.41, 144.00, 136.42, 134.63, 130.13, 128.19, 123.52, 120.30, 119.15, 115.99, 115.14, 99.50, 68.31, 59.93, 54.27, 49.68, 40.06, 39.97, 39.89, 39.80, 39.73, 39.63, 39.56, 39.47, 39.39, 39.30, 39.13, 38.97, 36.68, 13.48. HRMS (ESI+): m/z ($M+H^+$) calcd: 392.1835, found: 392.1914.

2-(4-{2-[2-(2,2,2-Trifluoro-ethyl)-2H-[1,2,4]triazol-3-yl]-4,5-dihydro-6-oxa-1,3a-diaza-benzo[e]azulen-8-yl}-pyrazol-1-yl)-ethanol (11g)

^{1}H NMR (500 MHz, DMSO-d_6) δ 8.34 (d, *J* = 8.3 Hz, 1H), 8.26 (s, 1H), 8.10 (s, 1H), 8.07 (s, 1H), 7.98 (s, 1H), 7.42 (dd, *J* = 8.3, 1.8 Hz, 1H), 7.29 (d, *J* = 1.7 Hz, 1H), 5.93 (q, *J* = 8.8 Hz, 2H), 4.95 (t, *J* = 5.3 Hz, 1H), 4.54 (td, *J* = 7.2, 1.7 Hz, 4H), 4.16 (t, *J* = 5.6 Hz, 2H), 3.77 (q, *J* = 5.6 Hz, 2H). ^{13}C NMR (126 MHz, DMSO-d_6) δ 156.03, 151.65, 149.58, 144.36, 144.33, 136.49, 134.95, 134.93, 129.84, 129.11, 128.25, 126.98, 124.76, 124.51, 122.53, 120.25, 119.29, 116.02, 114.77, 99.49, 68.24, 59.91, 54.28, 49.80, 49.54, 49.27, 49.00, 40.06, 39.97, 39.90, 39.80, 39.73, 39.63, 39.61, 39.47, 39.40, 39.30, 39.13, 38.97. HRMS (ESI+): m/z ($M+Na^+$) calcd: 468.1372, found: 468.1384. Melting point: 237 ºC.

2-(3-{4-[2-(2-Isopropyl-5-methyl-2H-[1,2,4]triazol-3-yl)-4,5-dihydro-6-oxa-1,3a-diaza-benzo[e]azulen-8-yl]-pyrazol-1-yl}-azetidin-1-yl)-ethanol (11h)

^{1}H NMR (500 MHz, DMSO-d_6) δ 8.45 (s, 1H), 8.37 (d, *J* = 8.5 Hz, 1H), 8.03 (s, 1H), 7.89 (s, 1H), 7.41 (dd, *J* = 8.5, 1.7 Hz, 1H), 7.32 (d, *J* = 1.8 Hz, 1H), 5.94 – 5.75 (m, 1H), 4.97 (p, *J* = 6.9 Hz, 1H), 4.54 – 4.49 (m, 4H), 4.47 (t, *J* = 5.5 Hz, 1H), 3.76 – 3.71 (m, 2H), 3.46 – 3.38 (m, 4H), 2.59 (t, *J* = 6.0 Hz, 2H), 2.50 (dt, *J* = 3.5, 1.7 Hz, 7H), 1.47 (d, *J* = 6.5 Hz, 6H). ^{13}C NMR (126 MHz, DMSO-d_6) δ 158.24, 155.86, 147.30, 143.89, 136.76, 134.32, 130.28, 129.96, 126.91, 123.65, 120.82, 119.29, 116.18, 115.38, 99.48, 68.32, 61.10, 61.02, 59.42, 51.41, 49.88, 49.68, 40.07, 39.97, 39.90, 39.80, 39.73, 39.64, 39.57, 39.47, 39.44, 39.31, 39.14, 38.97, 22.34, 13.82. HRMS (ESI+): m/z ($M+H^+$) calcd: 497.2389, found: 497.2419.

(S)-2-Hydroxy-1-(3-{4-[2-(2-isopropyl-5-methyl-2H-[1,2,4]triazol-3-yl)-4,5-dihydro-6-oxa-1,3a-diaza-benzo[e]azulen-8-yl]-pyrazol-1-yl}-azetidin-1-yl)-propan-1-one (11i)

^{1}H NMR (500 MHz, DMSO-d_6) δ 8.46 (d, *J* = 2.7 Hz, 1H), 8.38 (d, *J* = 8.4 Hz, 1H), 8.12 (s, 1H), 7.89 (s, 1H), 7.42 (dd, *J* = 8.5, 1.7 Hz, 1H), 7.32 (d, *J* = 1.8 Hz, 1H), 5.89 – 5.78 (m, 1H), 5.34 – 5.24 (m, 1H), 5.21 (t, *J* = 6.3 Hz, 1H), 4.75 (dt, *J* = 20.3, 8.9 Hz, 1H), 4.60 – 4.49 (m, 5H), 4.42 – 4.31 (m, 1H), 4.23 – 4.12 (m, 2H), 2.26 (s, 3H), 1.47 (d, *J* = 6.5 Hz, 6H), 1.22 (d, *J* = 6.8 Hz, 3H). ^{13}C NMR (126 MHz, DMSO-d_6) δ 173.67, 173.54, 158.24, 155.85, 147.29, 143.86, 137.63, 137.60, 134.10, 130.29, 130.01, 127.68, 127.63, 123.68, 121.01, 119.33, 116.26, 115.49, 68.32, 65.88, 65.75, 58.08, 57.97, 55.09, 55.05, 50.17, 50.12, 49.89, 49.68, 40.06, 39.97, 39.89, 39.80, 39.73, 39.63, 39.56, 39.47, 39.40, 39.30, 39.13, 38.97, 22.38, 22.34, 22.33, 20.22, 13.82. HRMS (ESI+): m/z ($M+H^+$) calcd: 503.2519, found: 503.2603. Melting point: 166 ºC.

1-{4-[2-(2-Isopropyl-2H-[1,2,4]triazol-3-yl)-4,5-dihydro-6-oxa-1,3a-diaza-benzo[e]azulen-8-yl]-pyrazol-1-yl}-2-methyl-propan-2-ol (11j)

^{1}H NMR (500 MHz, DMSO-d_6) δ 8.38 (d, *J* = 8.3 Hz, 1H), 8.17 (s, 1H), 7.96 (s, 1H), 7.92 (d, *J* = 2.8 Hz, 2H), 7.40 (dd, *J* = 8.4, 1.7 Hz, 1H), 7.29 (d, *J* = 1.8 Hz, 1H), 5.91 (hept, *J* = 6.6 Hz, 1H), 4.76 (s, 1H), 4.53 (q, *J* = 5.8 Hz, 4H), 4.04 (s, 2H), 1.50 (d, *J* = 6.7 Hz, 6H), 1.10 (s, 6H). ^{13}C NMR (126 MHz, DMSO-d_6) δ 155.90, 150.19, 147.10, 144.05, 136.06, 134.62, 130.15, 130.01, 128.72, 123.78, 120.28, 119.27, 116.06, 115.20, 69.20, 68.32, 62.22, 50.24, 49.70, 40.06, 39.97, 39.90, 39.80, 39.73, 39.64, 39.56, 39.47, 39.40, 39.30, 39.13, 38.97, 27.23, 22.32. HRMS (ESI+): m/z ($M+H^+$) calcd: 434.2304, found: 434.2325. Melting point: 241 ºC.

1-{4-[2-(2-Isopropyl-5-methyl-2H-[1,2,4]triazol-3-yl)-4,5-dihydro-6-oxa-1,3a-diaza-benzo[e]azulen-8-yl]-pyrazol-1-yl}-2-methyl-propan-2-ol (11k)

^{1}H NMR (500 MHz, DMSO-d_6) δ 8.36 (d, *J* = 8.4 Hz, 1H), 8.17 (s, 1H), 7.96 (s, 1H), 7.89 (s, 1H), 7.39 (dd, *J* = 8.4, 1.8 Hz, 1H), 7.28 (d, *J* = 1.8 Hz, 1H), 5.94 – 5.72 (m, 1H), 4.76 (s, 1H), 4.57 – 4.44 (m, 4H), 4.04 (s, 2H), 2.26 (s, 3H), 1.47 (d, *J* = 6.7 Hz, 6H), 1.09 (s, 6H). ^{13}C NMR (126 MHz, DMSO-d_6) δ 158.24, 155.88, 147.30, 143.92, 136.05, 134.57, 130.27, 129.98, 128.71, 123.63, 120.28, 119.26, 116.05, 115.23, 99.49, 69.19, 68.31, 62.22, 49.87, 49.69, 40.06, 39.97, 39.90, 39.80, 39.73, 39.64, 39.60, 39.47, 39.40, 39.30, 39.13, 38.97, 27.23, 22.38, 22.35, 13.83. HRMS (ESI+): m/z ($M+H^+$) calcd: 448.2461, found: 448.2541.

2-{3-[2-(1-isopropyl-3-methyl-1H-1,2-4-triazol-5-yl)-5,6-dihydrobenzo[f]imidazo[1,2-d][1,4]oxazepin-9-yl]-1H-pyrazol-1-yl}-2-methylpropanamide (11l)

^{1}H NMR (500 MHz, DMSO) δ 8.42 (s, 1H), 8.37 (d, *J* = 8.3 Hz, 1H), 8.02 (s, 1H), 7.89 (s, 1H), 7.46 (dd, *J* = 8.3, 1.8 Hz, 1H), 7.36 (d, *J* = 1.8 Hz, 1H), 7.22 (s, 1H), 6.87 (s, 1H), 5.90 – 5.73 (m, 1H), 4.62 – 4.42 (m, 4H), 2.50 (dt, *J* = 3.6, 1.7 Hz, 5H), 2.26 (s, 3H), 1.74 (s, 6H), 1.47 (d, *J* = 6.5 Hz, 6H). ^{13}C NMR (126 MHz, DMSO) δ 173.78, 158.24, 155.88, 147.31, 143.94, 136.64, 134.60,

130.26, 129.88, 126.42, 123.62, 120.32, 119.31, 116.17, 115.26, 68.31, 64.48, 49.89, 49.70, 40.06, 39.97, 39.89, 39.80, 39.72, 39.63, 39.56, 39.47, 39.30, 39.13, 38.96, 25.47, 22.34, 13.82.HRMS (ESI+): m/z ($M+H^+$) calcd: 461.2413, found: 461.2427. Melting point: 259 ºC.

Characterization of Biochemical and Cellular Activity In Vitro.

Enzymatic activity of the Class I PI3K isoforms was measured using a fluorescence polarization assay that monitors formation of the product 3,4,5-inositoltriphosphate molecule as it competes with fluorescently labeled PIP3 for binding to the GRP-1 pleckstrin homology domain protein. An increase in phosphatidyl inositide-3-phosphate product results in a decrease in fluorescence polarization signal as the labeled fluorophore is displaced from the GRP-1 protein-binding site. Class I PI3K isoforms were purchased from Perkin-Elmer or were expressed and purified as heterodimeric recombinant proteins. Tetramethylrhodamine-labeled PIP3 (TAMRA-PIP3), di-C8-PIP2, and PIP3 detection reagents were purchased from Echelon Biosciences. PI3Kα was assayed under initial rate conditions in the presence of 10 mM Tris (pH 7.5), 25 μM ATP, 9.75 μM PIP2, 5% glycerol, 4 mM $MgCl_2$, 50 mM NaCl, 0.05% (v/v) Chaps, 1 mM dithiothreitol, 2% (v/v) DMSO at 60 ng/mL. After assay for 30 min at 25 ºC, reactions were terminated with a final concentration of 9 mM EDTA, 4.5 nM TAMRA-PIP3, and 4.2 μg/mL GRP-1 detector protein before reading fluorescence polarization on an Envision plate reader. IC_{50}'s were calculated from the fit of the dose-response curves to a 4-parameter equation. Each reported value is an average of 3 experiments and all had a standard deviation less than one geometric mean.

Analysis of total and phosphorylated Akt.

Tris lysis buffer containing 150mM NaCl, 20mM Tris PH 7.5, 1mM EDTA, 1mM EGTA, 1% Triton X-100, phosphatase inhibitor 1 (Sigma P2850), phosphatase inhibitor II (Sigma P5726), protease inhibitor (Sigma P8340), 1mM NaF, and 1mM PMSF was added to frozen tumor biopsies. Tumors were dissociated with a

small pestle (Konte Glass Company 749521-1500), sonicated briefly on ice, and centrifuged at maximum RPM for 20 minutes at 4C. 5-20ug of protein from tumor lysates was used to determine phosphorylation status. Samples were assayed in duplicates per manufacturer's protocol for pAkt/tAkt (MesoScale Discovery K11100D-2).

Proliferation assay with MCF7–neo/HER2 cells

Cell lines were obtained from the American Type Culture Collection (ATCC, Manassas, VA). MCF7-neo/HER2 ectopically expresses HER2 in the MCF7 parental cell line and was developed at Genentech.[26] Cell lines were cultured in RPMI supplemented with 10% fetal bovine serum, 100 units/mL penicillin, and 100 μg/mL streptomycin, 10 mM HEPES, and 2 mM glutamine at 37 ºC under 5% CO_2. MCF7-neo/HER2 cells or PC3 cells were seeded in 384-well plates in media at 1000 cells/well or 3000 cells/well, respectively, and incubated overnight prior to the addition of compounds to a final DMSO concentration of 0.5% v/v. MCF7-neo/HER2 cells were incubated for 3 and 4 days, respectively, prior to the addition of CellTiter-Glo reagent (Promega) and reading of luminescence using an Analyst plate reader. For anti-proliferative assays, a cytostatic agent such as aphidicolin and a cytotoxic agent such as staurosporine were included as controls. Dose-response curves were fit to a 4-parameter equation and relative IC_{50}'s were calculated using Assay Explorer software.

Liver Microsomal Incubation:

LMs (0.5 mL at 20 mg/mL) were pre-mixed with alamethicin dissolved in methanol (100 μg/mg of LMs), G6P dehydrogenase (2.88 units/mg LMs), and KPi buffer to a final volume of 5 mL. The cofactor mixture was prepared by adding NADP (3.33 mg/mL; 4 mM), UDPGA (12.92 mg/mL; 20 mM), G6P (6.8 mg/mL) and GSH (6.15 mg/mL; 20 mM) to 1 mL of 100mM KPi incubation buffer. Equal volumes of cofactor solution and LMs solution (2 mg/mL) were added and pre-incubated for 5 minutes at 37 □C. The reaction

was initiated by adding an equal volume of **3** (5 μM final concentration) in buffer for a final concentration of 0.5 mg/mL of LMs. Final concentration for was 5 mM for GSH and 1 mM for NADP. Following 1 hour of incubation at 37□C, the reaction was quenched by the addition of acetonitrile, followed by centrifugation at 3400 □ g for 10 minutes. The supernatant was transferred and evaporated. The samples were reconstituted in 10% acetonitrile in water.

Liquid chromatography (LC) equipment consisted of a LC-10AD pump from Shimadzu Corporation (Columbia, MD), a HTS PAL autosampler from CTC Analytics (Carrboro, NC), a series 1100 model 1315 DAD UV detector (Serial No. 11112915) from Agilent (Waldbronn, Germany), and a QTRAP®4000 mass spectrometer equipped with a TurboIonSpray® from Applied Biosystems (Foster City, CA). Various MS/MS functionalities were used for analysis, which included full scans, product-ion scans, and multiplereaction monitoring data-dependent ion (MRM ida) scans in positive-ion electrospray mode. The LC column was a Synergi Hydro-RP C18 (4 micron; 150 × 2.00 mm) from Phenomenex. (Torrance, CA). Mobile phase A was 0.1% formic acid in water and mobile phase B (MPB) was 0.1% formic acid in acetonitrile.

In vitro hepatocyte metabolite identification assays:

Cryopreserved hepatocytes from male Sprague-Dawley rat (RH; Lot MTN) and male beagle dog (DH; Lot OES) were purchased from Celsis/In Vitro Technologies (Baltimore, MD). Cryopreserved human hepatocytes (HH, pooled of 50 mixed gender; Lot Hup 58 mix) were purchased from CellzDirect (Pittsboro, NC). Mobile phase solvents 0.1% formic acid in water (Cat No 34673; Lot 82630) and 0.1% formic acid in acetonitrile (Cat No. 34668; Lot 82690) were purchased from Fluka (St. Louis, MO). InVitroGRO HT thawing medium (Product No. Z99019; Lot C01020C) was purchased from Celsis/In Vitro Technologies. DMEM medium (Cat No. 31053; Lot 719700) was purchased from Invitrogen/Gibco (Grand Island, NY). Cryopreserved hepatocytes were thawed using pre-warmed InVitroGRO HT thawing medium

in 50-mL centrifuge tubes. The tubes were centrifuged for 5 minutes at 80 × g and the supernatants were discarded. Cells were re-suspended with 50 mL of pre-warmed DMEM medium by gently inverting the tube several times. The tubes were centrifuged for 5 minutes at 80 × g and the supernatants were discarded. Cells were brought up in 2.5 mL of pre-warmed DMEM incubation medium. The total cell count and the number of viable cells were determined by the Trypan Blue exclusion method. Incubations were carried out in scintillation vials containing 0.5 mL of hepatocyte suspension ($2.2–2.6 \times 10^6$ cells/mL) and 0.5 mL of DMEM media containing test article (20 □M). The scintillation vials were placed on an orbital shaker rotating at 16 rpm in a humidified incubator at 37°C, 5% CO_2. The reaction was quenched with 4 mL of acetonitrile at 0 and 3 hours. Diclofenac (10 μM) was the positive control and was incubated with cryopreserved hepatocytes under the same conditions used for GDC-0032. The disappearance of diclofenac over 3 hours was monitored and the half-life of the compound was within expected values for each species.

In Vivo Xenograft Studies.

In vivo efficacy was evaluated in the MCF7-neo/Her2 xenograft model. Five million cells per mouse were resuspended in a 1:1 mixture of Hank's Buffered Salt Solution and Matrigel Basement Membrane Matrix (No. 356237, BD Biosciences; Santa Cruz, CA), and implanted into number 2/3 mammary fat pad of female athymic (nu/nu) nude mice obtained from Taconic (Hudson, NY). Prior to cell inoculation, 17-*β*-estradiol (0.36 mg/pellet, 60-day release, No. SE-121) obtained from Innovative Research of America (Sarasota, FL) were implanted into the dorsal shoulder blade area of each nude mouse. After implantation of cells, tumors were monitored until they reached a mean tumor volume of 250-350 mm^3 prior to initiating dosing. Test articles were dissolved in 0.5% methylcellulose with 0.2% Tween-80 (MCT) and administered daily via oral (PO) gavage.

Tumor volumes were determined using digital calipers (Fred V. Fowler Company, Inc., Newton, MA) using the formula (L x W x W)/2. Tumor growth inhibition (TGI) was calculated as the percentage of

the area under the fitted curve (AUC) for the respective dose group per day in relation to the vehicle, such that %TGI = 100 x (1 – ($AUC_{treatment}$/day)/($AUC_{vehicle}$/day)). Curve fitting was applied to Log_2 transformed individual tumor volume data using a linear mixed-effects (LME) model with the R package nlme, version 3.1-97 in R v2.13.0 (R Development Core Team 2008; R Foundation for Statistical Computing; Vienna, Austria).[27] Tumor sizes and body weights were recorded twice weekly over the course of the study. Mice with tumor volumes ≥ 2000 mm^3 or with losses in body weight ≥ 20% from their weight at the start of treatment were euthanized per IACUC guidelines.

For pharmacodynamic marker analysis, MCF7-neo/HER2 xenograft tumors were excised from animals and immediately snap frozen in dry ice.

ABBREVIATIONS USED/KEYWORDS

PI3K, phosphoinositide 3-kinase; PTEN, phosphatase and tensin homologue; PIP2, 4,5-phospatidylinositolbisphosphate; PIP3, 3,4,5-phosphatidylinositoltrisphosphate; mTOR, mammalian target of rapamycin; RTK, receptor tyrosine kinase; LogD, logarithm of the distribution coefficient; TGI, tumor growth inhibition; HLM, human liver microsome; MLM, mouse liver microsome; HH, human hepatocyte.

AUTHOR INFORMATION

° Current address: OncoMed, 800 Chesapeake Drive, Redwood City CA 94063.

Corresponding authors:

* C.O.N.: Phone: +1-(650)-225-2923; Email: chudin@gene.com;

* T.P.H: Phone: +1-(650)-467-3214; Email: theffron@gene.com

ACKNOWLEDGMENTS

We are grateful to Joe Lyssikatos, James Crawford, Travis Remarchuk and Jae Chang (Genentech) for helpful discussions and critical reading of the manuscript. We thank Chris Hamman, Mengling Wong, Baiwei Lin, Yanzhou Liu and Deven Wang for purification and analytical support. Technical support from Hoa Le and Sashi Gopaul are also acknowledged.

REFERENCES

(1) Vivanco, I.; Sawyers, C. L. The phosphatidylinositol 3-Kinase AKT pathway in human cancer *Nature Rev. Cancer* **2002**, *2*, 489–501.

(2) Cantley, L. C. The phosphoinositide 3-kinase pathway *Science* **2002**, *296*, 1655–1657.

(3) Campbell, I.; Russell, S.; Choong, D.; Montgomery, K.; Ciavarella, M.; Hooi, C.; Cristiano, B.; Pearson, R.; Phillips, W. Mutation of the PIK3CA gene in ovarian and breast cancer *Cancer Res.* **2004**, *64*, 7678–7681.

(4) Samuels, Y.; Wang, Z.; Bardelli, A.; Silliman, N.; Ptak, J. High Frequency of Mutations of the PIK3CA Gene in Human Cancers *Science* **2004,** *304*, 554.

(5) Bertelsen, B.; Steine, S.; Sandvei, R. Molecular analysis of the PI3K-AKT pathway in uterine cervical neoplasia: Frequent PIK3CA amplification and AKT phosphorylation *Int. J. Cancer* **2006**, *118*, 1877–1883.

(6) Byun, D.; Cho, K.; Ryu, B.; Lee, M.; Park, J.; Chae, K.; Kim, H.; Chi, S. Frequent monoallelic deletion of PTEN and its reciprocal associatioin with PIK3CA amplification in gastric carcinoma *Int. J. Cancer* **2003**, *104*, 318–327.

(7) Shuttleworth, S. J.; Silva, F. A.; Cecil, A. R. L.; Tomassi, C. D.; Hill, T. J.; Raynaud, F. I.; Clarke, P. A.; Workman, P. Progress in the Preclinical Discovery and Clinical Development of Class I and Dual Class I/IV Phosphoinositide 3-Kinase (PI3K) Inhibitors *Curr. Med. Chem.* **2011**, *18*, 2686–2714.

(8) Jarvis, L. M. PI3K At The Clinical Crossroads *Chem. & Eng. News* **2011**, *89*, 15-19.

(9) Staben, S. T.; Siu, M.; Goldsmith, R.; Olivero, A. G.; Do, S.; Burdick, D. J.; Heffron, T. P.; Dotson, J.; Sutherlin, D. P.; Zhu, B.-Y.; Tsui, V.; Le, H.; Lee, L.; Lesnick, J.; Lewis, C.; Murray, J. M.; Nonomiya, J.; Pang, J.; Prior, W. W.; Salphati, L.; Rouge, L.; Sampath, D.; Sideris, S.; Wiesmann, C.; Wu, P. Structure-based design of thienobenzoxepin inhibitors of PI3-kinase *Bioorg. Med. Chem. Lett.* **2011**, *21*, 4054–4058.

(10) Heffron, T. P.; Wei, B.; Olivero, A.; Staben, S. T.; Tsui, V.; Do, S.; Dotson, J.; Folkes, A. J.; Goldsmith, P.; Goldsmith, R.; Gunzner, J.; Lesnick, J.; Lewis, C.; Mathieu, S.; Nonomiya, J.; Shuttleworth, S.; Sutherlin, D. P.; Wan, N. C.; Wang, S.; Wiesmann, C.; Zhu, B.-Y. Rational Design of Phosphoinositide 3-Kinase α Inhibitors That Exhibit Selectivity over the Phosphoinositide 3-Kinase β Isoform *J. Med. Chem.* **2011**, *54*, 7815–7833.

(11) Staben, S. T.; Blaquiere, N.; Bradley, E.; Kolesnikov, A.; Do, S.; Heffron, T. P.; Lesnick, J.; Murray, J.; Nonomiya, J.; Olivero, A. G.; Pang, J.; Salphati, L.; Wei, B.; Wu, P. Cis-amide isosteric replacement in thienobenzoxepin inhibitors of PI3-kinase *Bioorg. Med. Chem. Lett* **2013**, *23*, 897-901.

(12) Staben, S. T.; Ndubaku, C.; Blaquiere, N.; Belvin, M.; Bull, R. J.; Dudley, D.; Edgar, K.; Gray, D.; Heald, R.; Heffron, T. P.; Jones, G. E.; Jones, M.; Kolesnikov, A.; Lee, L.; Lesnick, J.; Lewis, C.; Murray, J.; McLean, N. J.; Nonomiya, J.; Olivero, A. G.; Ord, R.; Pang, J.; Price, S.; Prior, W. W.; Rouge, L.; Salphati, L.; Sampath, D.; Wallin, J.; Wang, L.; Wei, B.; Wiesmann, C.; Wu, P. Discovery of thiazolobenzoxepin PI3-kinase inhibitors that spare the PI3-kinase β isoform *Bioorg. Med. Chem. Lett.* **2013**, *23*, 2606-2613.

(13) Folkes, A. J.; Ahmadi, K.; Alderton, W. K.; Alix, S.; Baker, S. J.; Box, G.; Chuckowree, I. S.; Clarke, P. A.; Depledge, P.; Eccles, S. A.; Friedman, L. S.; Hayes, A.; Hancox, T. C.; Kugendradas, A.; Lensun, L.; Moore, P.; Olivero, A. G.; Pang, J.; Patel, S.; Pergl-Wilson, G. H.; Raynaud, F. I.; Robson, A.; Saghir, N.; Salphati, L.; Sohal, S.; Ultsch, M. H.; Valenti, M.; Wallweber, H. J. A.; Wan, N. C.; Wiesmann, C.; Workman, P.; Zhyvoloup, A.; Zvelebil, M. J.; Shuttleworth, S. J. The Identification of 2-(1*H*-Indazol-4-yl)-6-(4-methanesulfonyl-piperazin-1-ylmethyl)-4-morpholin-4-yl-thieno[3,2-*d*]pyrimidine (GDC-0941) as a Potent, Selective, Orally Bioavailable Inhibitor of Class I PI3 Kinase for the Treatment of Cancer *J. Med. Chem.* **2008**, *51*, 5522–5532.

(14) Smith, D. A.; Di, L.; Kerns, E. H. The effect of plasma protein binding on in vivo efficacy: misconceptions in drug discovery *Nat. Rev. Drug Discov* **2010**, *9*, 929–939.

(15) Sutherlin, D. P.; Bao, L.; Berry, M.; Castanedo, G.; Chuckowree, I.; Dotson, J.; Folks, A.; Friedman, L.; Goldsmith, R.; Gunzner, J.; Heffron, T.; Lesnick, J.; Lewis, C.; Mathieu, S.; Murray, J.; Nonomiya, J.; Pang, J.; Pegg, N.; Prior, W. W.; Rouge, L.; Salphati, L.; Sampath, D.; Tian, Q.; Tsui, V.; Wan, N. C.; Wang, S.; Wei, B.; Wiesmann, C.; Wu, P.; Zhu, B.-Y.; Olivero, A. Discovery of a Potent, Selective, and Orally Available Class I Phosphatidylinositol 3-Kinase (PI3K)/Mammalian Target of Rapamycin (mTOR) Kinase Inhibitor (GDC-0980) for the Treatment of Cancer *J. Med. Chem.* **2011**, *54*, 7579–7587.

(16) Sutherland, J. J.; Raymond, J. W.; Stevens, J. L.; Baker, T. K.; Watson, D. E. Relating Molecular Properties and in Vitro Assay Results to in Vivo Drug Disposition and Toxicity Outcomes *J. Med. Chem.* **2012**, *55*, 6455–6466.

(17) The $cLogD_{7.4}$ values were calculated using MoKa® Software (version 1.1.0, Molecular Discovery).

(18) Blaquiere, N.; Do, S.; Dudley, D.; Folkes, A. J.; Heald, R.; Heffron, T.; Jones, M.; Kolesnikov, A.; Ndubaku, C.; Olivero, A. G.; Price, S.; Staben, S.; Wang, L. Benzoxazepin PI3K Inhibitor Compounds and Methods of Use *PCT Int. Appl.* **2011**, WO/2011036280/A1.

(19) Iddon, B.; Lim, B. L. Reactions of 1,2-dimethylimidazole, particularly its metallation *J. Chem. Soc., Perkin Trans. 1* **1983**, 271–277.

(20) Bellina, F.; Cauteruccio, S.; Rossi, R. Efficient and Practical Synthesis of 4(5)-Aryl-1*H*-imidazoles and 2,4(5)-Diaryl-1*H*-imidazoles via Highly Selective Palladium-Catalyzed Arylation Reactions *J. Org. Chem.* **2007**, *72*, 8543–8546.

(21) Martinelli, J.R.; Freckmann, D.M.M.; Buchwald, S.L Convenient Method for the Preparation of Weinreb Amides via Pd-Catalyzed Aminocarbonylation of Aryl Bromides at Atmospheric Pressure *Org. Lett.* **2006**, *8*, 4843-4846.

(22) Hammerich, O. Anodic Oxidation of Hydrocarbons *Organic Electrochemistry (4th Edition)* **2001**, 471-498.

(23) Cruciani, G.; Carosati, E.; De Boeck, B.; Ethirajulu, K.; Mackie, C.; Howe, T.; Vianello, R. MetaSite: understanding metabolism in human cytochromes from the perspective of the chemist *J. Med. Chem.* **2005**, *48*, 6970–6979.

(24) Detailed information provided in the Experimental Section.

(25) Data from additional pharmacokinetic experiments, human dose predictions and preclinical safety assessments conducted with **11l** will be the subject of future reports.

(26) Wallin, J. J.; Guan J.; Prior, W. W.; Lee, L. B.; Berry, L.; Belmont, L. D.; Koeppen, H.; Belvin, M.; Friedman, L. S.; Sampath, D. GDC-0941, a novel class I selective PI3K inhibitor, enhances the efficacy of docetaxel in human breast cancer models by increasing cell death in vitro and in vivo *Clin. Canc. Res.* **2012**, *18*, 3901-3911.

(27) Wallin, J. J.; Edgar, K. A.; Guan, J.; Berry, M.; Prior, W. W.; Lee, L.; Lesnick, J. D.; Lewis, C.; Nonomiya, J.; Pang, J.; Salphati, L.; Olivero, A. G.; Sutherlin, D. P.; O'Brien, C.; Spoerke, J. M.; Patel, S.;

Lensun, L.; Kassees, R.; Ross, L.; Lackner, M. R.; Sampath, D.; Belvin, M.; Friedman, L. S. GDC-0980 is a novel class I PI3K/mTOR kinase inhibitor with robust activity in cancer models driven by the PI3K pathway *Mol. Canc. Ther.* **2011**, *10*, 2426-2436.

Table of contents graphics